Palaeogeography, Palaeoclimatology, Palaeoecology 565 (2021) 110189

Contents lists available at ScienceDirect

Palaeogeography, Palaeoclimatology, Palaeoecology

journal homepage: www.elsevier.com/locate/palaeo

Invited research article

The impact of cyclical, multi-decadal to centennial climate variability on arsenic sequestration in lacustrine sediments

B.R.B. Gregory [a,*,1], R.T. Patterson [a], J.M. Galloway [a,b], E.G. Reinhardt [c]

[a] Ottawa-Carleton Geoscience Center and Department of Earth Sciences, Carleton University, 1125 Colonel By Dr., Ottawa, ON K1S 5B6, Canada
[b] Geological Survey of Canada, 3303 33rd St. NW, Calgary, AB T2L 2A7, Canada
[c] School of Geography and Earth Sciences, McMaster University, 1280 Main St. W., Hamilton, ON K1S 5B6, Canada

ARTICLE INFO

Editor: Shucheng Xie

Keywords:
Itrax-XRF
Wavelet analysis
Spectral analysis
Solar cycles
Pacific Decadal Oscillation
Arctic Oscillation

ABSTRACT

Examining paleoclimate-driven changes of elemental contaminants, such as Arsenic (As), increases the understanding of the mobility and fate of elements under a warming climate scenario. To characterize the variability in As sequestration in the sediments of a freshwater system in response to decadal- to centennial-scale climate oscillations, a freeze-core (CON01) was recovered from Control Lake, Northwest Territories. Radiocarbon dating of 13 bulk-organic samples provided temporal reference to core depth. Sediment geochemistry was determined using Itrax X-ray fluorescence core-scanning (Itrax-XRF). Elemental concentrations were measured on a sub-set of samples using ICP-MS after multi-acid (MA) digestion to assess the accuracy of Itrax-XRF results through a multivariate log-ratio (MLC) calibration. Comparison of Itrax-XRF to ICP-MS using the MLC in ItraXelerate software show Pearson's R^2 values >0.75, with the exception of As (R^2 = 0.44). MLC-calibrated Itrax-XRF elemental data were centered log-ratio (CLR) transformed to eliminate issues related to data closure. During the ca. 3300-yr sedimentary record, moderate-strength negative correlations between As_{CLR} and K_{CLR} (Spearman's $\rho = -0.38$, *p-value* < 0.001, $n = 785$), and As_{CLR} and Ti_{CLR}, (Spearman's $\rho = -0.52$, *p-value* < 0.001, $n = 785$) suggest that As is primarily sequestered in sediments during intervals of warmer temperatures and higher productivity. Proxies for sediment particle size (Ti_{CLR}, K_{CLR}) and As concentration (As_{CLR}) were examined for response to quasi-periodic climate oscillations using spectral analysis. Significant periodicities were observed with approximately 4–13, 30–60, 90–120, and 160–280 yr periods in Ti_{CLR}, K_{CLR}, and As_{CLR} records. These frequencies are interpreted as corresponding to the North Atlantic Oscillation and/or 8–14-yr Schwabe sunspot cycles, 30–60-yr Pacific Decadal Oscillation, and centennial-scale solar cycles (e.g., 90-yr Gleissberg cycle; 205-yr Suess cycle). Coeval occurrence of these periodicities revealed through wavelet analysis of Control Lake geochemistry data suggests that these climate cycles only impact Control Lake when they occur concurrently.

1. Introduction

Lacustrine systems serve as semi-permanent storage for metal(loid) contaminants (Becker et al., 2001; Keimowitz et al., 2005; Macdonald et al., 2005; Bai et al., 2010; Bing et al., 2011; Bowell et al., 2014). Changes in redox state, pH, or availability of adsorbents in these environmental systems can induce the release of previously sequestered contaminants (Martin and Pedersen, 2002; Keimowitz et al., 2005; Bai et al., 2010; Miller et al., 2019, 2020). Climate can be a major control of the redox conditions of lacustrine systems by climate-driven mediation of temperature and precipitation that, in turn, affect nutrient delivery and surface water temperature, and thus primary production and redox setting. These changes lead to increased autochthonous productivity, shifts in the duration and stability of seasonal thermal stratification, and the duration of winter ice cover during which degradation of organic matter (OM) consumes oxygen in the system (e.g., Wetzel, 2001; Quesada et al., 2006; Snortheim et al., 2017; Palmer et al., 2019). In reducing environments, redox-sensitive elements, such as arsenic (As), can be released from sediments to overlying waters through the reductive dissolution of minerals, particularly Fe-oxy(hydro)oxides, in the lake sediments (Schuh et al., 2018; Palmer et al., 2019). Conversely, As can be incorporated into sulfides in shallow sediments under reducing

* Corresponding author.
E-mail addresses: braden.gregory@carleton.ca (B.R.B. Gregory), tim.patterson@carleton.ca (R.T. Patterson), jennifer.galloway@canada.ca (J.M. Galloway), ereinhar@mcmaster.ca (E.G. Reinhardt).
[1] Present address: Department of Biology, University of Ottawa, Marie-Curie Private, Ottawa, ON K1N 9A7, Canada.

https://doi.org/10.1016/j.palaeo.2020.110189
Received 15 July 2020; Received in revised form 14 December 2020; Accepted 17 December 2020
Available online 24 December 2020

conditions (Schuh et al. 2018; Miller et al., 2020). These processes are likely mediated by organic matter (Galloway et al., 2018). Future climate variability is predicted to impact primary production, and thus, will impact chemical stability, transportation, and sequestration of metal(loids) (Macdonald et al., 2005; Galloway et al., 2018; Miller et al., 2019, 2020). It is imperative for effective environmental stewardship to better quantify the potential impact of paleoclimate on the mobility of elemental contaminants to understand their responses to on-going and future climate change.

Quasi-periodic shifts in sea surface temperature (SST) and sea-level pressure (SLP), and the resultant re-organization of global atmospheric circulation patterns through atmospheric teleconnections, control regional temperature and precipitation worldwide (Bonsal et al., 2006; Skinner et al., 2006; Sheffield and Wood, 2008; Deser et al., 2009; Zhang et al., 2010). By altering precipitation and temperature regimes, climate oscillations can directly or indirectly impact contaminant mobility, transport, and bioavailability. Although the possible changes in the concentration of chemical contaminants in response to climate change have been posited previously (see Macdonald et al., 2005 for a review of probable mechanisms), few studies have attempted to quantify this possible relationship. Most of the literature concerning this topic has focused on the response of mercury to climate oscillations (Outridge et al., 2007; Gratz et al., 2009; Rydberg et al., 2010; Loseto et al., 2015; Slemr et al., 2016), or the response of other non-metalloid contaminants (Eckhardt et al., 2003; Hung et al., 2005; Christoudias et al., 2012; Rigét et al., 2013). These studies are, however, limited by their relatively short, centennial-scale records that prevent recognition of the influence of multi-decadal to centennial climate oscillations. Millennial-scale paleoclimate records are needed to understand the response of elements of potential concern to sub-decadal to centennial-scale climate oscillations that affect the climate of much of North America.

Arsenic (As) is a contaminant of concern in the Northwest Territories (NT), where it naturally occurs in the mineralized shear zones of the Slave Geological Province and derived surficial materials. Previous work in the NT has shown that there is a strong relationship between lake productivity and As mobility between modern lake sediments and surface waters (Galloway et al., 2018; Van den Berghe et al., 2018; Palmer et al., 2019). Paleoclimate studies of NT lakes using sediment cores observed a similar relationship between productivity, temperature variations, sediment input into lacustrine systems, and As sequestration on centennial to millennial timescales (Gregory et al., 2019a; Miller et al., 2020). We posit that quasi-periodic climate oscillations that control temperature in the NT will impact lake productivity and sediment input into lacustrine systems, and that corresponding shifts in the geochemistry of lake sediment will impact As sequestration in these systems. To test these hypotheses, a freeze-core was recovered from Control Lake, NT, near geogenic sources of As. Control Lake is a small lake found within the mineralized shear zone of the Courageous Lake Greenstone Belt (CLGB) near the modern boreal-forest-tundra transition. Control Lake was chosen for detailed study because it occurs in a mineralized region where As concentrations are high relative to the Canadian Council of Ministers of the Environment Probable Effect Limit for As of 17 ppm (CCME, 2001; median [As] 123 ppm in Control Lake sediments). Near-total geochemical variations in sediment were determined using Itrax high-resolution core scanning x-ray fluorescence (Itrax-XRF) at sub-decadal resolution (median = 3.32 yr per datapoint). The relative geochemical change measured by Itrax-XRF analysis was converted to an estimate of actual geochemical variations through multivariate log-ratio calibration to ICP-MS data following 4-acid digestion after the methods recommended by Gregory et al. (2019b). Examination of the prominent frequencies in time series of K_{CLR}, Ti_{CLR}, and As_{CLR} are examined below using spectral analyses to characterize (1) whether known semi-periodic climate oscillations impact sediment geochemistry and (2) if the resultant change in sediment geochemistry impacts As sequestration in lake sediment.

2. Background

2.1. Climate variability in northern Canada

Documented climate variability in subarctic and Arctic Canada in the historical record corresponds to quasi-periodic oscillations in coupled ocean-atmosphere systems of the Atlantic, Pacific, and Arctic oceans. The North Atlantic Oscillation (NAO) and Arctic oscillation (AO) impact temperature and precipitation in the Canadian Arctic and Northeastern Canada (Buermann et al., 2003; Déry and Wood, 2005; Bonsal et al., 2006; Fauria and Johnson, 2006; Bonsal and Shabbar, 2011; Sarmiento and Palanisami, 2011). The NAO is defined by a significant difference in sea level pressure (SLP) between the Icelandic Low and the Azores high (Van Loon and Rogers, 1978). The AO is defined by persistent SLP anomalies across the entire Arctic (Thompson and Wallace, 1998). Because of the strong correspondence between the phase of NAO and AO, and the possibility that the NAO may be a spatially limited expression of the hemispherical AO (Deser, 2000; Dickson et al., 2002), the two oscillations will be discussed together hereafter. Temperature and precipitation patterns in Western and Central Canada are also influenced by Pacific Ocean oscillations including: El Niño/the Southern Oscillation (ENSO), and the Pacific Decadal Oscillation (PDO). El Niño/the Southern Oscillation is a fluctuation in SLP and sea surface temperature (SST) in the equatorial Pacific between Tahiti and South America (Wang and Picaut, 2004). The PDO is a variation in the position and strength of the Aleutian low and corresponding SST anomalies in the NE Pacific (Mantua and Hare, 2002). Both PDO and ENSO affect modern climate (Buermann et al., 2003; Déry and Wood, 2005; Bonsal et al., 2006; Fauria and Johnson, 2006; Bonsal and Shabbar, 2011; Sarmiento and Palanisami, 2011) and are documented in paleoecological records (Patterson et al., 2004a, 2004b; Chang and Patterson, 2005; Patterson et al., 2007; Babalola et al., 2013; Galloway et al., 2013; Patterson et al., 2013).

The periodicity and strength of climate oscillations are impacted by internal processes inherent to the ocean-atmosphere system, as well as external forcing from solar activity (Gray et al., 2016; Newman et al., 2016). Several authors have observed variations in prevailing patterns of AO/NAO, PDO, and ENSO in response to short term cycles in total solar irradiance that correspond to 8–14-yr cycles (Schwabe cycle) in sunspot frequency and longer-term variation in the intensity of this cycle at ca. 88-yr period (Gleissberg cycle) and ca. 205-yr period (Suess/De Vreis cycle; Christoforou and Hameed, 1997; Patterson et al., 2004a, 2005, 2013; Meehl et al., 2008; Van Loon et al., 2012; Galloway et al., 2013; Gray et al., 2013, 2016; Scaife et al., 2013; Ólafsdóttir et al., 2013; Dalton et al., 2018; Veretenenko and Ogurtsov, 2019). Although there is controversy regarding the mechanisms that allow relatively minor changes in solar insolation (1–2 W m^{-2} at the top of the atmosphere in the tropics; Lean et al., 2005) to alter oceanic and atmospheric circulation patterns, modeling efforts suggest that solar insolation plays a role in altering oceanic and atmospheric systems (Meehl et al., 2008, 2009; Gray et al., 2010). Moreover, typical SST and SLP anomalies associated with oceanic-atmospheric oscillations are observed to change when examining periods in-phase with peaks in solar variability (e.g., Roy and Haigh, 2010, 2012; Van Loon and Meehl, 2016). Variations in temperature and precipitation within the study area may thus be expected to respond to solar forcing, ocean-atmospheric oscillations, or a combination of internal and external forcing. These climate-oscillation induced variations in temperature and precipitation have been observed to impact environmental systems indirectly through modifying forest fire frequency, river and lake hydrology, lake productivity, and freeze-up and break-up dates of lakes/rivers (Bonsal et al., 2001; Dickson et al., 2002; Buermann et al., 2003; Déry and Wood, 2005; Bonsal et al., 2006; Fauria and Johnson 2006; Sarmiento and Palanisami, 2011; Galloway et al., 2013; Patterson et al., 2013; Vincent et al., 2015; Dalton et al., 2018).

2.2. Previous work on Control Lake

Previous paleolimnological research was conducted by Miller et al. (2020) on a 44 cm (ca. 2100 calibrated years BP [cal yr BP]) Glew core recovered from Control Lake in winter, 2016. Miller et al. (2020) analyzed As speciation in pore water and sediments, bulk sediment geochemistry, sediment particle size, type of organic matter in sediment based on Rock-Eval Pyrolysis, and detailed mineralogical examination of sediment using SEM mineralogical liberation analysis, electron microprobe analysis, and bulk X-ray absorption near-edge spectrometry. Miller et al. (2020) observed that As is predominantly associated with Fe-oxy(hydr)oxides in the lake sediment, with minor proportions of As found in authigenic framboidal pyrite, and trace amounts associated with allogenic arseno-sulphides eroded and transported into the lake. Based on the comparison of As concentration and mineralogy to variations in particle size and organic matter type, Miller et al. (2020) inferred that warmer conditions resulted in greater autochthonous productivity, increasing labile organic material available for degradation and promoting dysoxic/anoxic conditions near the lake bed. The low-oxygen conditions induced the reductive dissolution of As-bearing minerals, resulting in the incorporation of As into pyrite formed in reducing the sediment.

Further paleolimnological study of Control Lake was conducted by Gregory et al. (2019a) who examined changes in ICP-MS-derived As concentrations in lake sediment and the corresponding response of micro-organisms (Arcellinida) on a ca. 133 cm (ca. 4500 cal yr BP) freeze core (CON02) recovered during winter 2016 alongside Miller et al. (2020). Arcellinida is a group of amoebae that build a shell from mineral particles in the environment. Previous work in the NT has shown that Arcellinida respond strongly to variations in As concentration in lake sediment and can be used to re-create down-core variations in As concentration (Gavel et al., 2018; Nasser et al., 2020), particularly useful as As is diagenetically mobile. Comparison of As concentration to shifts in the Arcellinida community of Control Lake showed that As was

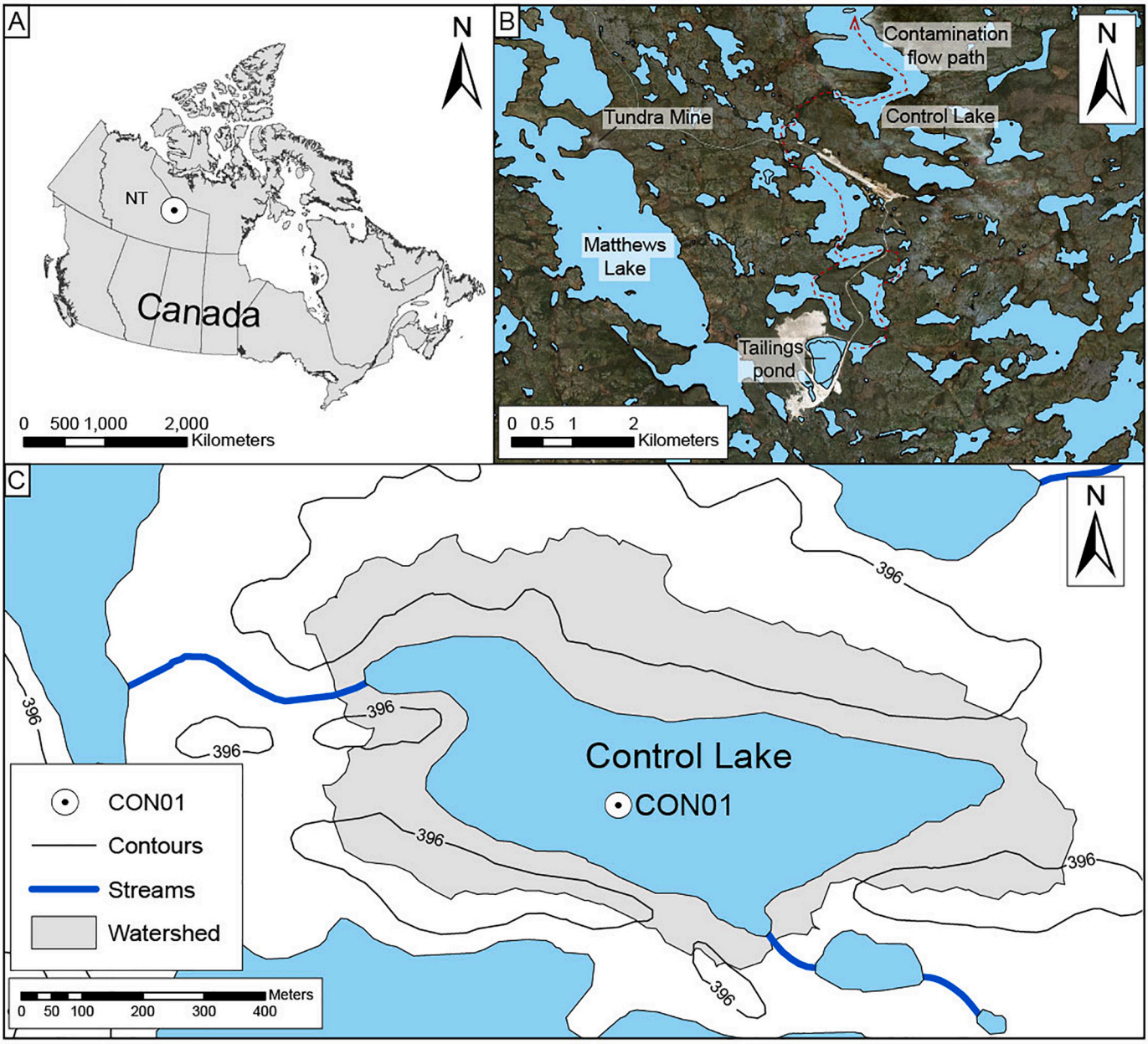

Fig. 1. Study area showing (A) location of Control Lake in the Northwest Territories (NT), Canada, (B) Control Lake in the context of the Tundra/Salmita Mine and surrounding lake systems, and (C) the Control Lake watershed and outflow to adjacent lakes.

likely post-depositionally mobile, or else not a primary stressor on Arcellinida during the Holocene (Gregory et al., 2019a). The extended paleoclimate archive recorded a major change in sediment geochemistry at ca. 2500 cal yr BP interpreted to be a shift from boreal forest to tundra setting (Gregory et al., 2019a).

2.3. Study area

Control Lake is located approximately 240 km NE of Yellowknife, NT. Modern vegetation surrounding Control Lake consists of grasses and low tundra shrubs (Seabridge Gold Inc., 2010; AANDC, 2013). The region is characterized by gradually undulating topography consisting of glacially-scoured bedrock hummocks and glacial-till filled swales (McCurdy and McNeil, 2014). Control Lake is underlain by a veneer of glacial till 2–10 m thick resting on ca. 2.6 Ga low-grade phyllite and slate of the Yellowknife Supergroup (Moore, 1986; Padgham, 1992; Thompson and Kerswill, 1994; Tetra Tech Wardrop, 2012; McCurdy and McNeil, 2014). Gold deposits were recognized near Courageous Lake in 1939, and the Tundra/Salmita mine was soon after established adjacent to Matthews Lake and west of Control Lake (Fig. 1B). Extraction and processing of ores occurred on-site between 1964 and 68 and again from 1983 to 86 (Silke, 2009; AANDC, 2013). Recent monitoring of the Tundra/Salmita mine property showed Control Lake does not contain anomalously high metal concentrations relative to other lakes on the property, suggesting it has not been impacted by mining in the region (AANDC, 2013; Miller et al., 2019). It is, therefore, a suitable system for assessing the possible impact of natural climate variations on geogenic As sequestration in a climatically sensitive area with geogenic sources of As and a site of concern for future As mobility.

Control Lake is relatively small (surface area = 23.4 Ha) and shallow (Z_{max} = 5 m). Recent monitoring of Control Lake during open-water seasons showed circum-neutral pH (6.10–7.62) and conductivity values ranging from 11.4 to 18.3 SpC. Hydrological modeling of Control Lake has revealed a small watershed that drains the surrounding glacially-scoured hollow with two stream outflows to the west and south-east (Fig. 1C). Hydrological monitoring at the Tundra/Salmita mine property indicates that the region receives a relatively low yearly average precipitation (213 mm) (Seabridge Gold Inc., 2010). The sub-arctic tundra experiences short summers and long winters, with typical freeze-up of lakes near Control Lake occurring in late September, and spring break-up of ice-cover occurring in June (AANDC, 2013). The average daily temperature is −9.2 °C in the region, but can vary between −43 to 6 °C yearly (Seabridge Gold, 2010).

3. Methods

Core CON01 (length = 103 cm) was collected in March 2016, through the ice at the approximate Z_{max} of Control Lake using a single-faced freeze corer (64.07771°N, −111.13493°W, 429 m above sea level; Fig. 1). Frozen sediment was removed from the freeze cores, wrapped in clingfilm in the field and shipped frozen to Carleton University, where it was stored at −25 °C. Upon arrival at Carleton University, freeze cores were cleaned, photographed, and sediment stratigraphy was described.

3.1. Radiocarbon dating

Radiocarbon dating of lake sediment provided temporal reference to core depth. Thirteen bulk sediment sub-samples of approximately 2 mL were collected using ceramic and stainless-steel instruments from CON01. Samples were analyzed at the A.E. Lalonde AMS facility at the University of Ottawa following a triple acid wash (Table 1). Radiocarbon dates were calibrated to years before present (cal yr BP) using the terrestrial radiocarbon curve IntCal13 (Reimer et al., 2013). An age-depth model was generated using the Bayesian Age Calibration (BACON) package for R statistical software (Blaauw and Christen, 2019; R Core Team, 2019) based on the calibrated radiocarbon dates (Fig. 2).

Table 1
Radiocarbon results for analysis of bulk organic sediment from Control Lake core CON01 showing uncalibrated age (^{14}C yr BP) and the fraction of modern carbon ($F^{14}C$).

Lab ID	Core depth (cm)	^{14}C yr BP	Error	$F^{14}C$	Error
UOC-3555	1–2	Modern	38	1.0386	0.0049
UOC-2107	2–4	Modern	21	1.0109	0.0026
UOC-3556	10–11	1276	38	0.8531	0.0040
UOC-3557	18–19	1336	38	0.8468	0.0040
UOC-2108	27–27.5	1304	21	0.8505	0.0022
UOC-3558	37–38	1868	38	0.7926	0.0038
UOC-3559	47–48	1942	38	0.7852	0.0037
UOC-3560	56–57	2529	38	0.7299	0.0034
UOC-2109	65–65.5	2252	22	0.7561	0.0020
UOC-3561	73.5–74.5	2489	38	0.7336	0.0035
UOC-3562	83.5–84.5	3020	38	0.6866	0.0032
UOC-3563	91.5–92.5	2879	38	0.6988	0.0033
UOC-2110	97–97.5	3297	21	0.6640	0.0017

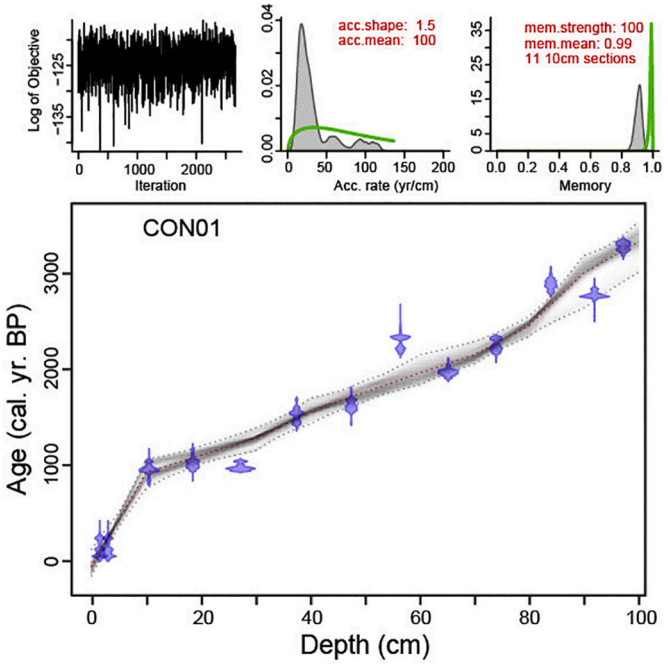

Fig. 2. Age-depth relationships for the Control Lake sediment core CON01 based on 13 AMS radiocarbon dates on bulk organic material, modelled using BACON. Radiocarbon dates and error are shown in blue, and inferred age in gray – darker areas suggest greater likelihood of age at a given depth. The dashed black line shows the linear age model used for wavelet analysis. The bottom panel shows the age difference (cal. yr. BP) between the Bayesian age model (gray) and linear age model (red dashed line) with increasing depth in the core. (For interpretation of the references to colour in this figure legend, the reader is referred to the web version of this article.)

3.2. Geochemical analysis

Core CON01 was prepared for Itrax-XRF analysis following procedures outlined by Gregory et al. (2019b). Core CON01 was cut lengthwise using a ripsaw into an approximately 3-cm-wide section, then subdivided into nine approximately 12.5-cm-long slabs using a fine-bladed hacksaw. After sub-sectioning, core slabs were cleaned by gently warming the surface and removing the melted sediment by scraping the surface with clean glass microscope slides parallel to bedding direction. Core slabs were analyzed at the McMaster Core-Scanning facility using purpose-designed, insulated boxes (Gregory et al., 2019b). The sediment slabs were analyzed at 1 mm resolution using a Mo-anode for 25 s per interval at 25 kV and 22 mA. Sediment

cores were scanned in triplicate, initially at 1 mm resolution and subsequently at coarser resolution (every 5 mm). Sediment core slabs had to be returned to the freezer in between replicate scans to ensure core integrity.

3.3. Itrax-XRF data processing and comparison

Triplicate Itrax-XRF scans of CON01 were screened to remove invalid data, then loaded into the ItraXelerate software (v.1.0; Weltje et al., 2015). ItraXelerate was used to merge the triplicate scans, and automatically replace zeros (non-detects) with half of the lowest observed values for each given element; only elements with <30% non-detects were considered for analysis (Supplementary Table 1).

To ensure Itrax-XRF adequately detected elements of interest, ICP-MS analysis was conducted on the core slabs used for Itrax-XRF analysis. Nine elements of interest were selected from the dataset for comparison, including redox-sensitive elements (As, Fe, Mn, S), indicators of minerogenic input into the system (Ti, K), and elements abundant in surrounding glacial till (Ca, Cr, Cu). Core slabs were re-cleaned after Itrax analysis, and 1-cm long sub-samples were selected for analysis based on recommendations provided by the ItraXelerate automated sample selection algorithm. Six samples were analyzed in triplicate by ICP-MS to provide a measure of absolute geochemical error. Triplicate samples were taken from 3-cm long sub-samples due to limited material remaining in freeze core slabs. Sub-sampled material was sent to Acme/Bureau Veritas, Vancouver, for ICP-MS analysis following near-total multi-acid digestion (MA-ICP-MS; Supplementary Table 2). The average Relative Percent Difference (RPD) across the six triplicates for the nine elements selected for comparison in this study (As, Ca, Cr, Cu, Fe, K, Mn, Ti, S) ranged from 1.0 to 9.5% ($n = 27$). Titanium had the highest maximum RPD (17.1%), followed by Mn (14.5%); all remaining elements have maximum RPDs <10%. Two pulp duplicates of material analyzed by Bureau Veritas had an RPD of <7.4% (range = 0–7.4%) across all elements of interest. Two internal standards, OREAS25A-4A and OREAS45E, were analyzed in duplicate as a measure of the accuracy of the ICP-MS analysis. For standard OREAS25A-4A, all elements of interest were < 10% Relative Percent Error (RPE) of expected values (range = 0.9–9.4%). For OREAS45E standard, RPE for elements of interest ranged from 0.2% to 16.6% ($n = 18$). Arsenic exhibited the highest RPE (16.6%), followed by K (14.2%), and Fe (9.8%). After MA-ICP-MS analysis, the ItraXelerate software was used to compare MA-ICP-MS to Itrax-XRF results using the Multivariate log-ratio Calibration (MLC) method proposed by Weltje et al. (2015). The depth tolerance of the MLC calibration was set to 15 mm in the ItraXelerate software to account for 3-cm-long subsamples analyzed in triplicate using in MA-ICP-MS.

3.4. Spectral and wavelet analysis

Following recommendations by Weltje et al. (2015), as well as others (Aitchison, 1999; Aitchison et al., 2000; Egozcue and Pawlowsky-Glahn, 2008; Filzmoser et al., 2009), geochemical data were interpreted using centered log-ratios (CLR). All elements in the calibrated dataset were normalized to the geometric mean of elemental concentrations at a given point, followed by taking the logarithm of the data (Supplementary Table 3). This transformation "opens" the

dataset to ensure none of the observed variations in elemental geochemistry were impacted by closed-sum effects. Additionally, CLR transformation minimizes the influence of specimen effects in Itrax-XRF data as data is normalized to the geometric mean of elemental concentration for a given point before log-transformation.

Prior to wavelet and spectral analyses, select elements were examined for paleoenvironmental significance. Common lithogenic elements were compared to coarse resolution particle size measured in the Glew core studied by Miller et al. (2020) that extends back to ca. 2100 cal yr BP. After CLR transformation of Itrax-XRF and particle size datasets, and removal of an outlier at 24 cm depth in the particle size dataset, both K_{CLR} and Ti_{CLR} are positively correlated with clay (Pearson's $R_{Ti\text{-}clay} = 0.28$, *p-value* = 0.06, $n = 46$; Pearson's $R_{K\text{-}clay} = 0.27$, *p-value* = 0.07, $n = 46$) and silt (Pearson's $R_{Ti\text{-}silt} = 0.33$, *p-value* = 0.03, $n = 46$; Pearson's $R_{K\text{-}silt} = 0.35$, *p-value* = 0.012, $n = 46$) and negatively correlated to sand (Pearson's $R_{Ti\text{-}sand} = -0.31$, *p-value* = 0.03, $n = 46$; Pearson's $R_{K\text{-}sand} = -0.30$, *p-value* = 0.05, $n = 46$).

Prior to carrying out wavelet and spectral analysis, CLR data were detrended by subtracting the loess-smoothed ($\alpha = 0.3$) trend. The uneven spacing of the age model necessitated the use of the REDFIT procedure for spectral analysis of data. As outlined by Schulz and Mudelsee (2002), a Lomb-Scargle Fourier Transformation was applied to a series of segments generated from the time series that overlap by 50%, with the penultimate spectrogram generated representing the average of the overlapping spectrograms. The significance of the spectrogram was assessed by comparing data to a null-model generated by 1000 Monte Carlo simulations of an AR(1) model; 99%, 95% and 90% confidence levels (CL) are provided as a measure of confidence in spectral signals. A Hanning window was used to reduce spectral leakage during Fourier transformation.

Wavelet transform of the data was used to examine shifts in periodicity over time (Torrence and Compo, 1998). Wavelet analysis was performed using the R-package Morlet (Bunn et al., 2018) that enables wavelet analysis of unevenly spaced data. Data were detrended by subtracting the loess-smoothed ($\alpha = 0.3$) trend from CLR data to emphasize the shorter-term oscillations that were of interest to this study and eliminate long-term variations that may have been influenced by edge effects. The Morlet wavelet was used as it represents a good compromise between frequency and time resolution. Statistical significance of the wavelet power was tested against 1000 Monte Carlo simulations of a red-noise model (AR(1)).

4. Results

4.1. Age model

The Control Lake sediment core (CON01) records 3271 +/− 263 cal yr BP of deposition. In this study, only the last 82 cm (2536 +/− 119 cal yr BP) was examined using spectral and wavelet analyses as a shift from boreal forest to tundra conditions occurred at ca. 2500 cal yr BP, with tundra conditions lasting until present day (Gregory et al., 2019a). Radiocarbon ages have an error of 21–38 years (Table 1). The age-depth model indicates that there was a nearly steady rate of sedimentation during deposition of CON01, with a slower sedimentation rate of ca. 0.1 mm/yr in the upper 10 cm of the core (10 yr/mm), followed by a relatively steady rate of ca. 0.44 mm/yr (2.23 yr/mm) for the remainder of the core (Table 1, Fig. 2). The 95% confidence interval of the age model based on monte carlo simulations ranges from 73 to 273 yr (median 113 yr, $n = 1001$). The median difference between datapoints in the time series is 9.7 r (mode = 10 yr, $n = 100$) years in the upper 10 cm were sedimentation rate is higher, and 2.7 yr (mode = 2 yr, $n = 900$) years for the remainder of the core that exhibits slower sedimentation rate.

4.2. Itrax-XRF calibration

Calibration of the Itrax-XRF data based on ICP-MS using a multivariate CLR calibration using the ItraXelerate software package showed strong correlations for most elements (Fig. 3). Calcium, Cr, Fe, K, Mn, and Ti had Pearson's R^2 values of >0.9. Copper and S showed weaker Pearson's R^2 values of 0.78 and 0.75, respectively. Arsenic exhibited the weakest correlation between the XRF and ICP-MS data at $R^2 = 0.44$. Comparison of the Itrax-XRF results, ICP-MS results carried out after multi-acid digestion (MA-ICP-MS; Supplementary Table 2) on core CON01 used in this study, and ICP-MS results following an *aqua-regia* digestion (AQ-ICP-MS) from adjacent core CON02 (Gregory et al., 2019a) indicate that volatilization of As was likely. However, As_{CLR} in CON01 exhibits similar trend to concentrations measured using AQ-ICP-

MS on CON02 (Spearman's ρ = 0.67, *p*-value <0.001, *n* = 75; Supplementary Fig. 1). The MA-ICP-MS shows lower As concentrations in sediment than the concentrations measured using AQ-ICP-MS for the adjacent and time equivalent core ($mean_{MA}$ = 75 ppm, *n* = 46; $mean_{AQ}$ = 121 ppm, *n* = 75). Calibrated Itrax-XRF results are also comparable between the cores, but lower concentrations of As occur in CON01 throughout the record. We thus have confidence that As_{CLR} reasonably accurately recreates As trends with the caveat that the magnitude of these oscillations may be an under-estimation of actual concentration changes.

Itrax-XRF As_{CLR} values show moderate strength, statistically significant, negative correlations to K_{CLR} (Spearman's ρ = −0.38, *p-value* < 0.001, *n* = 785) and Ti_{CLR}, (Spearman's ρ = −0.52, *p-value* < 0.001, *n* = 785). Ti_{CLR} and K_{CLR} show strong correlation to each other in core (Spearman's ρ = 0.90, *p-value* < 0.001, *n* = 785). These correlations are apparent in the trends in the three CLR-normalized elements in core CON01 (Fig. 4). There is a decreasing trend in As_{CLR} from ca. 2600 to ca. 2200 cal yr BP, followed by a highly variable, but overall increasing trend, from ca. 2200 to −66 cal yr BP (Fig. 4). Both Ti_{CLR} and K_{CLR} exhibit an increasing trend from ca. 2600 to ca. 2200 cal yr BP, followed by relatively high and variable values from ca. 2200 cal yr BP until ca. 1000 cal yr BP, then a gradual decrease from 1000 cal yr BP until modern day.

4.3. Spectral and wavelet analysis

Spectral analysis of CLR elements (K_{CLR}, Ti_{CLR}, As_{CLR}) shows peaks above the 99% CL. For As_{CLR}, periods at ca. 10 yr, ca. 87 yr, ca. 106–121 yr, and a broad peak from ca. 150 to 280 yr (max spectral power at 216 yr) were above the 99% CL (Fig. 5). An additional peak with a period of ca. 7 yr surpasses the 95% CL for As_{CLR}. Spectral analysis of K_{CLR} reveals frequencies of ca. 9 yr, ca. 12 yr, ca. 99–118 yr, ca. 140–150 yr, and ca. 216–243 yr above the 99% CL (Fig. 5). Two K_{CLR} spectral power peaks at ca. 11 yr and ca. 7 yr surpass the 95% CL. The spectrogram for Ti_{CLR} shows peaks in spectral power above the 99% CL with periods of ca. 9 yr, ca. 111–120 yr, ca. 140–170 yr, and ca. 205–280 yr as well as peaks with periods of ca. 7 yr, ca. 8.7 yr, ca. 11 yr, and ca. 12 yr that surpass the 95% CL.

Wavelet analysis of centered log-ratio data proxies indicates that periodicities are non-stationary throughout the sediment record of CON01. Wavelet analysis of As_{CLR} shows intermittent increases in spectral power with periods of 4–13 yr and ca. 16–30 yr that surpass the 95% CL (Fig. 6). Periods of ca. 28–44 yr and ca. 100–160 yr surpass the 95% CL threshold throughout the majority of the sedimentary record. From ca. 900–1350 cal yr BP and ca. 1770–2600 cal yr BP, regions of spectral power surpassing the 95% CL occur with periods of ca. 55–140 yr. In the intervening years (ca. 1350–1750 cal yr BP), the peak in

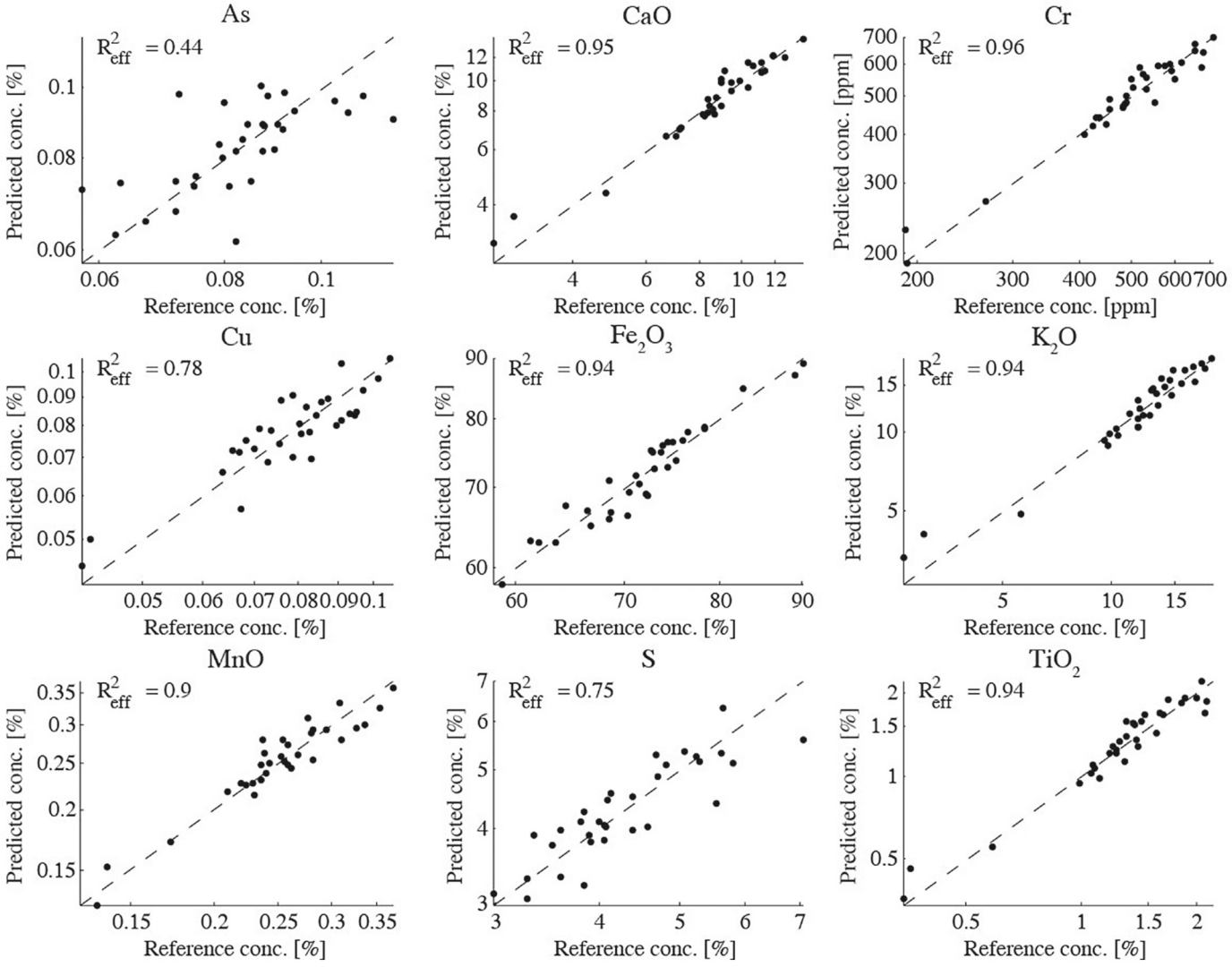

Fig. 3. Comparison of reference (MA-ICP-MS) and predicted concentrations (calibrated Itrax-XRF) results after calibration using multivariate centered log-ratio calibration.

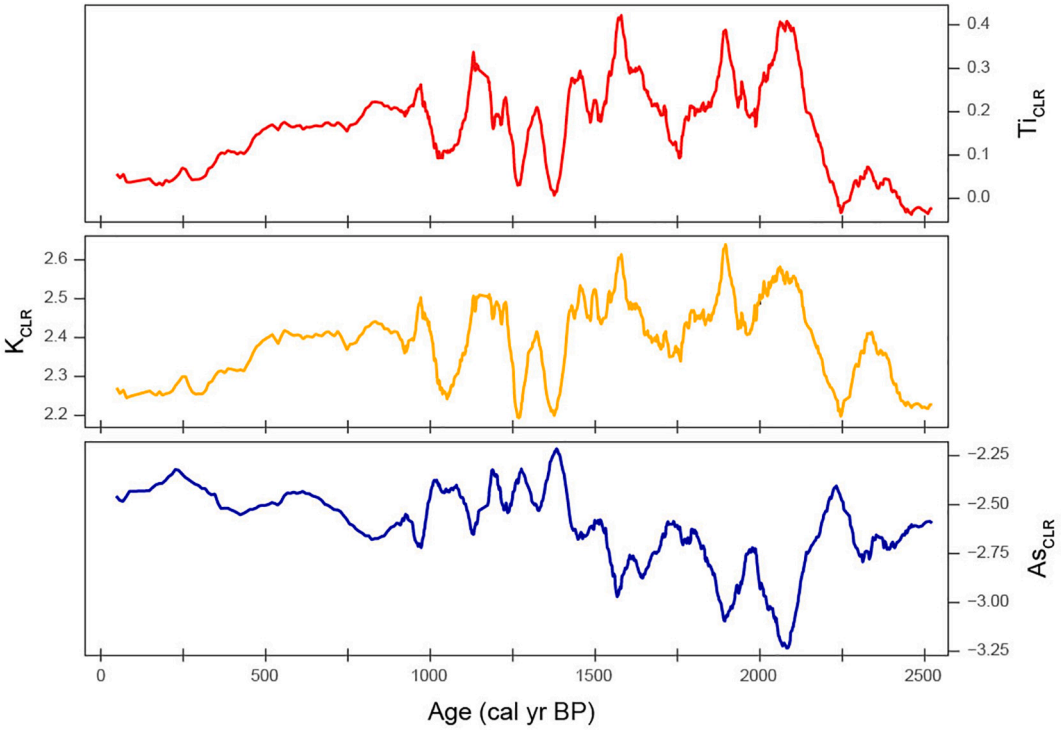

Fig. 4. Variations in Ti_{CLR} (red), K_{CLR} (yellow), and As_{CLR} (blue) trends during the last ca. 2500 cal. BP at Control Lake. Lines represent a 10-pt running mean of calibrated Itrax-XRF data. (For interpretation of the references to colour in this figure legend, the reader is referred to the web version of this article.)

spectral power with a periodicity of 55–140 yr diverges on the scalogram into two regions of high spectral power above the CL with periods of ca. 28–50 yr and ca. 130–160 yr, respectively.

The wavelet scalogram of K_{CLR} shows intervals of increased spectral power with periods of ca. 4–24 yr throughout the paleoclimate record (Fig. 7). Intervals of spectral power that surpass the 95% CL occur with periods of ca. 30–60 yr and ca. 70–165 yr throughout the record. As is observed in the wavelet scalogram of As_{CLR}, there is a broad region of high spectral power above the 95% CL with period of ca. 50–160 yr that occurs from ca. 850–1275 cal yr BP and ca. 1780–2300 cal yr BP. In the intervening interval (ca. 1275–1780 cal yr BP), the ca. 50–160 yr period signal diverges into two areas of high spectral power above the CL with periods of 30–60 yr and ca. 120–165 yr.

The Ti_{CLR} shows similar intervals of sporadic high spectral power at lower periods (ca. 4–13 yr). Intervals of high spectral power with periods of 28–55 yr and ca. 60–165 yr surpass the 95% CL throughout the majority of the paleoclimate record (Fig. 8). Between ca. 820–1320 cal yr BP and ca. 1790–2200 cal yr BP, high spectral power occurs with period of ca. 65–165 yr. From ca. 1320–1790 cal yr BP, high spectral power above the 95% CL occurs with period of ca. 28–60 yr and ca. 128–165 yr.

In the wavelet analysis of Ti_{CLR}, K_{CLR}, and As_{CLR}, there is an apparent stacking of significant periodicities wherein intervals of significance at lower-periods (e.g., ca. 4–8 yr) are coeval with intervals of significance at higher periods (ca. 16–20 yr, ca. 28–60 yr, ca. 60–100 yr; Figs. 6–8). Intervals of stacked periodicities occur at ca. 755–1010, ca. 1133–1249, ca. 1417–1590, ca. 1880–2040, and ca. 2250–2360 cal yr BP. Spectral analysis of these intervals corroborates the observations in wavelet analysis, with spectral peaks surpassing the 90% CL at ca. 4–13 yr, ca. 30 yr, 50 yr, and a broad peak in power encompassing ca. 100–300 yr (Fig. 9, Supplementary Fig. 2). The "stacking" intervals last an average of 146 yr (range = 84–256 yr, $n = 16$) and returned, on average, every 206 yr (range = 102–309, $n = 13$) between re-occurrence across for Ti_{CLR}, K_{CLR}, and As_{CLR} time series. Intervals that exhibit coeval occurrences of periodicities are more prominent in the K_{CLR} and Ti_{CLR} than in the As_{CLR} record.

5. Discussion

Prominent frequencies are discussed below using approximate ages. Despite the high resolution of radiocarbon dates in core CON01 (13 dates for 100 cm), there is inherent age-related uncertainties associated with the measurement of ^{14}C in sediment samples, the calibration of ^{14}C ages to cal yr BP, and in the creation of age models. The linear accumulation rate throughout the majority of CON01 provides confidence that the age model offers a reliable estimate of the actual age of sediments. Throughout most of CON01, there is a 2-yr difference between measured data points. Spectral signals are therefore pre-disposed to have even-numbered periods.

Throughout the record, the uneven spacing of the time series results in a variable Nyquist number, or the shortest possible spectral signal that can be reliably detected (Nyquist # = 2 x sample spacing). Between ca. -66 and 900 cal yr BP, a combination of rapid sedimentation rate (Nyquist number = 20 yr) and influence of edge effects limits the interpretability of wavelet analysis. During this interval, the relatively rapid sedimentation rate is likely caused by increased erosion in the catchment during this period as indicated by an increased proportion of sand-sized particles after ca. 1000 cal yr BP observed in Control Lake by Miller et al. (2020). From 2600 to 900 cal yr BP, a slower sedimentation rate allows for the interpretation of shorter periods <7 yrs. (Nyquist number = 4–6 yr).

Analysis of K_{CLR} and Ti_{CLR} time series revealed that there are significant periodicities in the window of ca. 200–240 yr, ca. 130–170 yr, ca. 99–120 yr, ca. 30–60 yr, and ca. 4–13 yr in both records. The As_{CLR} time series shares periodicities that overlap with those in the Ti_{CLR} and K_{CLR} records of ca. 150–280 yr, ca. 90–121 yr, ca. 30–55 yr, and ca. 4–13 yr Ti_{CLR} and K_{CLR} are inferred here to represent sediment delivery to Control Lake. As_{CLR} reflects changes As sequestration driven by shifts in the redox setting of lake waters and shallow sediments, or shifts in total As driven by increased sediment transport into Control Lake. Both

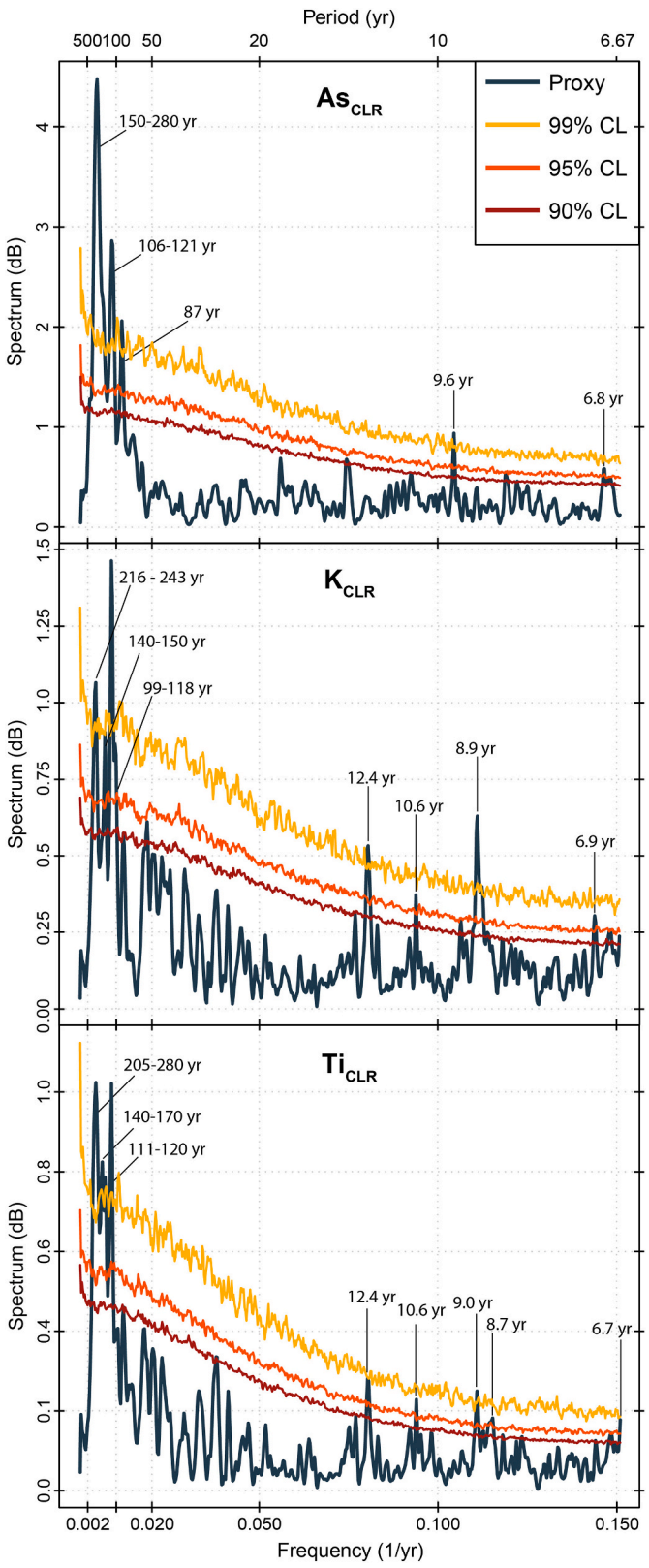

Fig. 5. Spectral analysis of As_{CLR}, Ti_{CLR} and K_{CLR} using redfit. Spectral power is shown in blue and confidence level (CL) based on red-noise models are shown in red (90%), orange (95%) and yellow (99%). (For interpretation of the references to colour in this figure legend, the reader is referred to the web version of this article.)

sediment delivery and redox setting can be influenced by temperature and precipitation. The length of winter ice coverage, snowpack thickness, and rate of spring melt are the primary controls on particle size and accumulation rate in tundra lake systems (Cuven et al., 2011; Amann et al., 2017; Macumber et al., 2018; Gregory et al., 2019a). Increases in air temperature and precipitation are therefore expected to impact the amount and coarseness of sediment transported into Control Lake. Temperature and precipitation may impact As secondarily through changes to lake depth and seasonal stratification regime, in-situ productivity, and/or the length of the open-water season. Together, these variables influence the redox conditions of the waters and shallow sediments (Wetzel, 2001; Quesada et al., 2006; MacDonald et al., 2009; Kraemer et al., 2017; Sinha et al., 2017; Snortheim et al., 2017) and can specifically affect As cycling in northern lakes whereby anoxic conditions develop under ice, stimulating reductive dissolution of As from shallow sediments (Palmer et al., 2019).

5.1. *Comparison of paleoclimate periodicities to known climate oscillations*

The As_{CLR}, Ti_{CLR}, and K_{CLR} time series show significant periodicities of ca. 4–13 yr in spectral analysis (Fig. 5). A ca. 4–16 yr periodicity is observed intermittently in the wavelet analyses of As_{CLR}, Ti_{CLR}, and K_{CLR} during the last ca. 2500 cal yr BP (Figs. 6–8). This short-period signal could correspond to several shorter-term climate oscillations with periods ranging from 2 to 14 yr (i.e., ENSO, NAO/AO, Schwabe sunspot cycles), or a combination of these phenomena. The lower margin of the ca. 4–13 yr. oscillations observed in spectral and wavelet analysis of Control Lake data approaches the upper limit of the typically observed range of ENSO periodicity of 2–7 yr. (Wang and Picaut, 2004). Paleoproxy records of ENSO variability indicate that the length of this periodicity may have been variable during the Holocene, with period length ranging up to 12 yrs. (Moy et al., 2002; McGregor and Gagan, 2004). The AO/NAO exhibits generally irregular periodicity over the historical record; however, some studies have suggested a prominent 2–10 yr periodicity in the AO/NAO indices (Hurrel and Loon, 1997; Rossi et al., 2011; Massei et al., 2007; Wanner et al., 2001; Ólafsdóttir et al., 2013). The Schwabe sunspot cycle exhibits a periodicity ranging from 8 to 14 yr (Solanki et al., 2004), overlapping with the observed period of ca. 4–13 yr.

Although changes in solar insolation due to Schwabe sunspot cycles are relatively minor, historical observations have shown that small-scale shifts in solar activity affect global climate (Meehl et al., 2009; Gray et al., 2010). A response to minor changes in solar insolation has also been observed in global climate models (Kodera and Kuroda, 2002; Meehl et al., 2008; Simpson et al., 2009; Misios et al., 2016, 2019). The response of climate to minor changes in solar insolation is posited to be the result of an increase in shallow-SST in cloud-free regions in the tropical Pacific that strengthens atmospheric circulation at the intertropical convergence zone/South Pacific convergence zone (Meehl et al., 2008; Misios et al., 2016, 2019). Alternatively, increases in solar UV-radiation impact stratospheric temperature profiles, ozone production, and the strength of Brewer-Dobson circulation that ultimately alters tropospheric and ocean temperature/circulation patterns (Kodera and Kuroda, 2002; Simpson et al., 2009). Variations in insolation induced by sunspot activity could impact the temperature and precipitation in the study area by altering global-scale atmospheric and oceanic circulation patterns.

It is possible that the ca. 4–13 yr period observed at Control Lake represents the combined effects of ENSO, AO/NAO and Schwabe cycles. Modeling and observational records have shown that the Schwabe sunspot cycle influences the AO/NAO such that stronger effects are felt when the oscillations are in phase (Van Loon et al., 2012; Osterberg et al., 2014; Thiéblemont et al., 2015; Van Loon and Meehl, 2016). Some studies have found AO/NAO circum-arctic SLP and SST anomalies are only present when the oscillation is in phase with the Schwabe sunspot

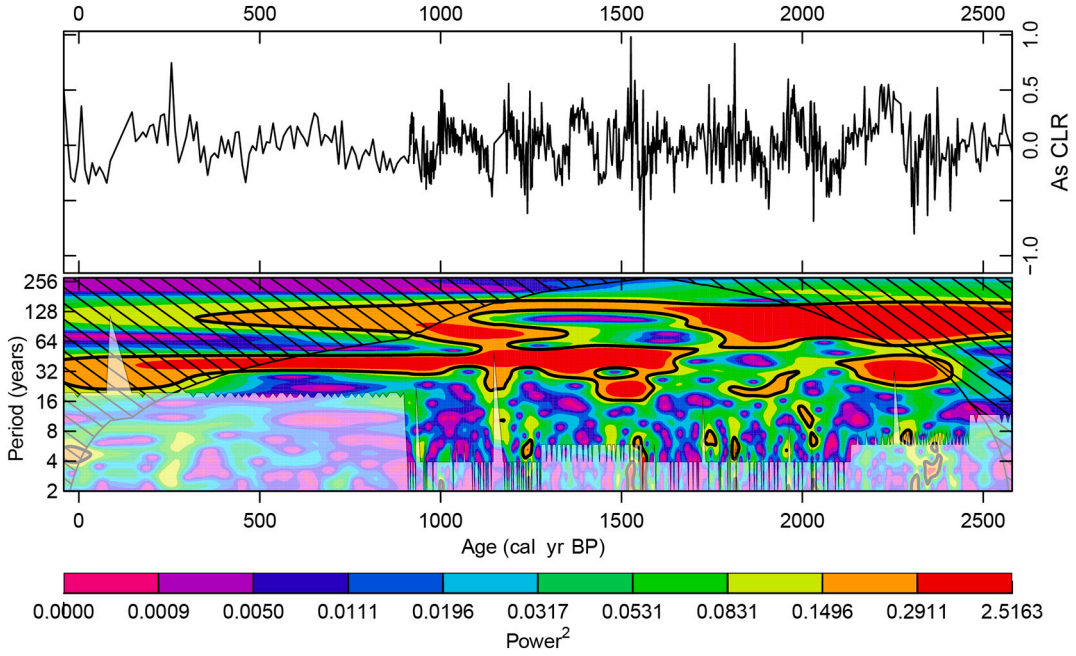

Fig. 6. The transformed As_{CLR} signal subject to wavelet transformation (top box) and the wavelet scalogram of As_{CLR} (bottom box). Areas that are significantly different (<95% CL) from a red noise model are indicated by thick black lines. The cone of influence (COI) is shown by black hatched area. Areas below the Nyquist number are indicated by translucent white overlay. Warm (cool) colors indicate higher (lower) power of the wavelet transformation. (For interpretation of the references to colour in this figure legend, the reader is referred to the web version of this article.)

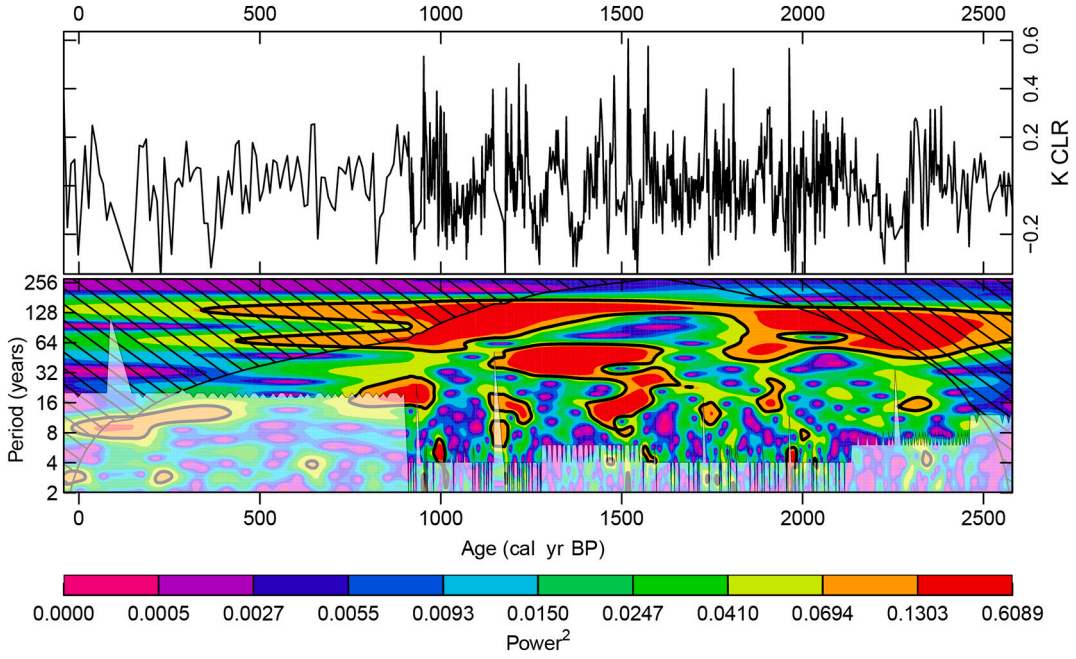

Fig. 7. The transformed K_{CLR} signal subject to wavelet transformation (top box) and the wavelet scalogram of K_{CLR} (bottom box). Areas that are significantly different (<95% CL) from a red noise model are indicated by thick black lines. The cone of influence (COI) is shown by black hatched area. Areas below the Nyquist number are indicated by translucent white overlay. Warm (cold) colors indicate higher(lower) power of the wavelet transformation. (For interpretation of the references to colour in this figure legend, the reader is referred to the web version of this article.)

cycle (Kodera, 2002; Kodera and Kuroda, 2005; Hood and Soukharev, 2012). Bonsal et al. (2006) also observed changes in the extent of AO/NAO-forced low-pressure excursions into north-central Canada during ENSO+ phases, which suggests that ENSO-induced ocean-atmospheric changes alter the extent to which the AO/NAO influences climate in western North America, including the continental NT. The short-period oscillations observed in the sediment geochemical record of the Control Lake record thus likely reflect a complex interplay of signal amplification and suppression between ENSO, AO/NAO and solar forcing at the Schwabe cycle temperature and precipitation of the central NT.

Wavelet analysis shows peaks in spectral power above the 95% CL, with periods of ca. 30–60 yr that are observed intermittently throughout the last ca. 2500 cal yr BP as concentration changes in the As_{CLR}, Ti_{CLR} and K_{CLR} records (Figs. 6–8). The observed ca. 30–60 yr period is

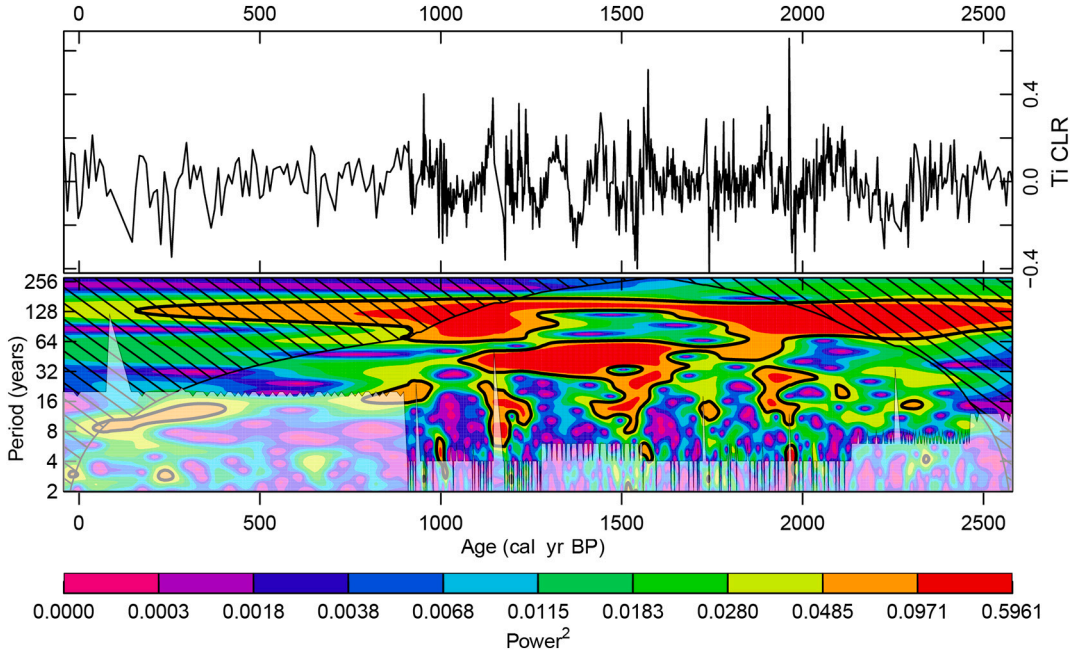

Fig. 8. The transformed Ti_{CLR} signal subject to wavelet transformation (top box) and the wavelet scalogram of Ti_{CLR} (bottom box). Areas that are significantly different (<95% CL) from a red noise model are indicated by thick black lines. The cone of influence (COI) is shown by black hatched area. Areas below the Nyquist number are indicated by translucent white overlay. Warm (cold) colors indicate higher(lower) power of the wavelet transformation. (For interpretation of the references to colour in this figure legend, the reader is referred to the web version of this article.)

interpreted to reflect the influence of the PDO on regional climate and geochemical change. The positive phase of the PDO is associated with warmer SST in the NE Pacific Ocean, a stronger and south-western positioned Aleutian Low-pressure system, and a more intense high-pressure system over much of the NT (Bonsal et al., 2001; Lapointe et al., 2017; Kren et al., 2016). These pressure cells result in the northward displacement of the polar jet, and a weakening of the stratospheric polar vortex, resulting in warmer, drier conditions in the central NT during a + PDO phase (Klein, 1949; Bonsal et al., 2001; Lapointe et al., 2017; Kren et al., 2016; Dalton et al., 2018). Warmer air temperature would result in shorter duration of winter ice cover and, in turn, increased autochthonous productivity during the lengthened open water season. A longer open-water season could impact sediment geochemistry by reducing the duration or intensity of dysoxia near the sediment-water interface. Warmer temperatures and drier conditions would result in more rapid spring-melt and delivery of relatively fine sediment to Control Lake or reduced sediment transport into the system (Cuven et al., 2011; Amann et al., 2017; Macumber et al., 2018).

Centennial and multi-centennial periodicities are present in the As_{CLR}, Ti_{CLR}, and K_{CLR} time series during the ca. 2500-yr sedimentary recorded at Control Lake. Spectral analysis of elemental time series shows prominent periodicities ca. 90–120 yr and ca. 150–280 yr (Fig. 5). Wavelet analysis shows peaks in spectral power above the CL with period of ca. 60–150 yr (Figs. 6–8). The ca. 90–120 yr periodicity observed in the Control Lake record may be related to the Gleissberg solar cycle, a long-term variation in the intensity of the Schwabe sunspot cycle (Gleissberg, 1971). Ogurtsov et al. (2002) observed ca. 50–80 yr and ca. 90–140 yr periodicities in this cycle based on an analysis of cosmogenic isotope records, direct observations (sunspots and auroral measurements), and paleoclimate proxies. The ca. 150–280 yr period present in spectral analysis of As_{CLR} and K_{CLR} corresponds to the Suess/De Vries cycle, a centennial-scale oscillation in solar intensity first observed in records of cosmogenic isotopes (^{14}C, ^{10}Be) and tree-ring thickness with a period of ca. 160–270 yr posited to be a modulation of 11-yr Schwabe cycles (Suess, 1980, 1986).

The Gleissberg and Suess solar cycles have been observed in paleoclimate records worldwide (Hodell et al., 2001; Wang et al., 2005; Raspopov et al., 2008; Pena et al., 2015; Liu et al., 2019), and paleoclimate records from NW North America. For example, the Gleissberg and Suess solar cycles were inferred to have influenced productivity and hydrology in a coastal fiord of mainland British Columbia with a period of ca. 82–89 yr and ca. 241–243 yr (Galloway et al., 2013). Gleissberg- and Suess-like oscillations were also observed in the diatom-based productivity records of Danny's Lake, in the central NT (Dalton et al., 2018), and Arolick Lake, Alaska (Hu et al., 2003). Timoney et al. (1997) observed centennial-scale oscillations in the flood-history of the Peace-Athabasca flood plain in Northern Alberta that are attributable to Gleissberg cycles. Wiles et al. (2004) observed shifts in glacial extent corresponding to variations in changes in total solar irradiance over centennial timescales. Widespread recognition of cycles in paleoclimate data on Gleissberg- and Suess frequencies across NW North America suggests these that periodic changes in solar intensity are an important control on climate.

Gleissberg and Suess solar cycles likely influence the climate of the central NT through altering the prevailing ocean-atmospheric patterns and thus the regional influence of the AO/NAO and PDO. Recent examinations of historical SST and SLP trends provided evidence of Gleissberg cycles impacting the intensity of the PDO (Meehl et al., 2008; Van Loon and Meehl, 2016). Similarly, Shen et al. (2006) observed a 50–80 yr period in the oscillatory pattern of the PDO index. Several researchers have observed variations in the oceanic and atmospheric patterns induced by the PDO caused by 11-yr sunspot cycles within the historical record (Kren et al., 2016) or a PDO-like response to solar forcing (Van Loon and Meehl, 2008, 2011). Hood and Soukharev (2012) observed AO-like response in global climate models in response to 11 yr solar cycles and several studies have noted an apparent solar influence on the AO/NAO on 11-yr timescales (Boberg and Lundstedt, 2002; Van Loon et al., 2012; Scaife et al., 2013; Gray et al., 2016; Smith et al., 2016; Van Loon and Meehl, 2016). Examination of modern trends in the atmospheric response to solar cycles showed statistically significant AO/NAO-like variations only during intervals of increased solar irradiance (Hood et al., 2013). Van Loon et al. (2012) documented variations in the influence of Schwabe solar cycles on the NAO depending on the phase of the Gleissberg cycle.

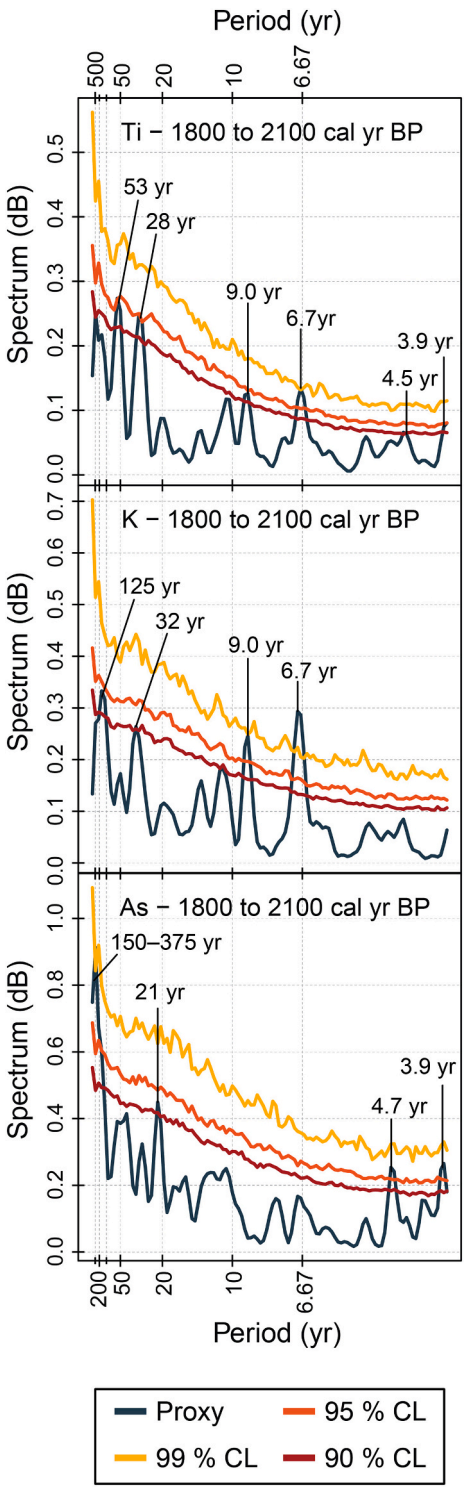

Fig. 9. Spectral analysis a subset of the entire As_{CLR}, Ti_{CLR} and K_{CLR} time series using redfit. Spectral power is shown in blue and confidence level based on red-noise models are shown in red (90%), orange (95%) and yellow (99%). (For interpretation of the references to colour in this figure legend, the reader is referred to the web version of this article.)

Sub- to multi-decadal periodicities in the As_{CLR}, Ti_{CLR} and K_{CLR} time series occur coeval with each other during several intervals in the CON01 record creating a stacking pattern in the wavelet scalograms (Figs. 6–8). The coeval occurrence of multiple signals during a given time interval in wavelet scalograms of paleoclimate records influenced by solar variability has been previously observed in records of diatom productivity in NT (Dalton et al., 2018), in productivity and sedimentation records from coastal British Colombia (Galloway et al., 2013; Patterson et al., 2013), in pollen spectra from east Asia (Xu et al., 2015; Park, 2017) and in precipitation records from China (Chu et al., 2014; Zhang et al., 2018). The stacking of signals suggests that the cumulative effect of multiple solar or internal climate phenomena is only sufficient to influence the environment of Control Lake when multiple oscillatory climate patterns are in-phase.

5.2. *Paleoclimate controls on As sequestration at Control Lake*

Late Holocene climate change impacted the sedimentology of Control Lake through changes in the hydrology of the catchment. Negative correlations between K_{CLR}, Ti_{CLR}, and As_{CLR} suggests that processes that increased delivery of fine sediment into the lake basin resulted in reduced As sequestration at Control Lake. Studies of varved Arctic lakes have shown that higher K and Fe concentrations correspond to intervals of gradual sedimentary deposition during winter ice-coverage and that elevated Ti concentrations are generally associated with increased silt deposition during spring snowmelt (Cuven et al., 2010; Amann et al., 2017). Furthermore, an increase in snowpack thickness and cooler conditions during snowpack melt correspond to increased sediment accumulation in Arctic lakes (Cockburn and Lamoureux, 2008; Cuven et al., 2011; Amann et al., 2017). Elevated values of Ti_{CLR} and K_{CLR} may thus represent thicker winter snowpack, prolonged snowpack melt driven by cooler temperatures, or extended ice coverage during winter. An increase in sediment transport into Control Lake may be expected to increase transportation of detrital As minerals into the lake, especially considering As is commonly associated with fine-grained Fe-oxy(hydr) oxides. However, the negative correlation between K and Ti and As suggests that variations in sediment input into Control Lake is not the primary mechanism controlling As sequestration. It is possible that extended periods of winter ice coverage during cooler intervals (higher K_{CLR}) increased the duration of reducing conditions in the shallow sediment and overlaying water column (Palmer et al., 2019). Anoxic conditions would release As sequestered in shallow sediment through reductive dissolution of Fe and Mn-oxy(hydr)oxides. Conditions that increase transport of geogenic As into Control Lake are thus also conditions that discourage the sequestration of As in shallow lake sediment.

Previous work in the NT has shown that increased labile organic matter in lake sediment can increase As sequestration because the labile organic matter encourages the microbial activity that mediates mineralization of As- and Fe-sulphides, and because the labile organic matter offers greater surface area for metal(loid) complexation (Galloway et al., 2018; Miller et al., 2020). During intervals of warmer temperatures and extended open-water season (Lower K_{CLR}, Ti_{CLR}), higher authigenic productivity would encourage As sequestration in shallow sediment through increasing the proportion of labile organic matter in the sediment. Furthermore, shorter duration of seasonal ice-cover (lower K_{CLR}) would minimize As loss through the reductive dissolution of Fe/Mn-oxy (hydr)oxides by reducing the length of, or degree of dysoxia in the shallow sediment. The combination of decreased As cycling in shallow sediment through reduced reductive dissolution of Fe-oxy(hydr)oxides, and the increase in labile organic matter together encourage As sequestration in Control Lake.

It is difficult to ascertain whether variations in sedimentary As concentrations at Control Lake represent depositional signals or early diagenesis. Miller et al. (2020) observed that Fe-oxy(hydr)oxides were the predominant hosts of As in Control Lake sediment, with minor proportions of As associated with framboidal pyrites. Typically, Fe-oxy (hydr)oxides are only stable under oxidizing conditions and are, therefore, not expected to be stable at depth in the sediment column under anoxic conditions (Schuh et al. 2018; Miller et al., 2020). The prevalence of As sorbed to Fe-oxy(hydr)oxides may be indicative of at least partial in-situ preservation of an As signal, however, the presence of authigenic framboidal pyrites indicates that redox conditions resulted in the

dissolution and re-precipitation of As minerals to some degree. Although temperature-induced variations in autochthonous productivity could influence As concentrations in lake sediment, it is unclear whether these trends represent a primary response to climate or whether shallow sediment horizons with grater concentrations of labile organic matter are more conducive to authigenic mineralization of As during early diagenesis. Regardless, our results indicate that warmer conditions with extended open-water seasons results in higher sequestration of As in shallow Arctic lakes, either during deposition or early diagenesis.

6. Conclusions

A sediment core collected from Control Lake, NT, was analyzed at sub-decadal resolution using Itrax-XRF to reconstruct the impact of quasi-periodic ocean-atmospheric oscillations on lacustrine geochemistry during the last ca. 2500 cal yr BP. Spectral and wavelet analysis of Ti_{CLR}, K_{CLR}, and As_{CLR} show that there was a response of lake sedimentation and hydrology to climate oscillations with periods of ca. 4–13 yr, ca. 30–60 yr, ca. 90–120 yr, and ca. 150–280 yr, corresponding to ENSO, AO/NAO, PDO, and solar cycles (Schwabe, Gleissberg, Suess). The geochemical response to climate oscillations was stronger when several periodicities occurred coevally. Variations in As_{CLR} show decadal- and centennial-scale oscillations that negatively correlate to changes in proxies for sedimentary input into Control Lake (K_{CLR} and Ti_{CLR}), suggesting a link between temperature-dependent shifts in hydrology and productivity, and long-term sequestration of As in sediment of shallow Arctic lakes. Although previous work found As was predominantly hosted in Fe-oxy(hydr)oxides, possibly representing depositional of As in oxic settings, it is unclear if shifts in As sequestration represent changes in As input or organic mediated mineralization of As during early diagenesis in the sedimentary record.

Supplementary data to this article can be found online at https://doi.org/10.1016/j.palaeo.2020.110189.

Declaration of competing interest

The authors declare that they have no known competing financial interests or personal relationships that could have appeared to influence the work reported in this paper.

Acknowledgments

We gratefully acknowledge funding for this research provided by a Polar Knowledge Canada grant to RTP and JMG (Grant #1516-149), Natural Resources Canada Clean Growth Program grant to RTP (Grant # CPG-17-0704), NSERC Discovery grant to RTP (Grant # RGPIN-2018-05329), Canadian Foundation of Innovation Infrastructure operating grant from EGR (Grant # 2003785), ArcticNet (Project 51 to JMG), the Geological Survey of Canada's Environmental Geoscience Program Metal Mining Project (Michael Parsons), Northern Baselines Activity (JMG) and a Geological Society of America Graduate Student Research Grant to BRBG. This manuscript represents NRCan contribution number/Numéro de contribution de RNCan: 20200575. We thank Dr. Elizabeth Anderson-Patterson for helping to refine the paper for submission. Thank you to Crown-Indigenous Relations and Northern Affairs Canada (Murray Somers and Joel Gowman) for access to the study site, and for substantial in-kind contributions that made collection of materials for research possible. Thank you to Michael Parsons (GSC Halifax), Clare Miller (University of Tasmania), Hendrik Falck (Northwest Territories Geological Survey), Andrew Macumber (Carleton University) and the staff of Delta Engineering and Nahanni Construction for their support during northern fieldwork.

References

Aboriginal Affairs and Northern Development Canada, 2013. Water Balance Monitoring at the Tundra Mine Site: 2012 Update, 101 pages.
Aitchison, J., 1999. Logratios and natural laws in compositional data analysis. Math. Geol. 31 (5), 563–580.
Aitchison, J., Barcelo-Vidal, C., Martin-Fernandez, J.A., Pawlowsky-Glahn, V., 2000. Logratio analysis and compositional distance. Math. Geol. 32 (3), 271–275.
Amann, B., Lamoureux, S.F., Boreux, M.P., 2017. Winter temperature conditions (1670–2010) reconstructed from varved sediments, western Canadian High Arctic. Quat. Sci. Rev. 172, 1–14.
Babalola, L.O., Patterson, R.T., Prokoph, A., 2013. Foraminiferal evidence of a late Holocene westward shift of the Aleutian Low. J. Foraminifer. Res. 43 (2), 127–142.
Bai, J., Yang, Z., Cui, B., Gao, H., Ding, Q., 2010. Some heavy metals distribution in wetland soils under different land use types along a typical plateau lake, China. Soil Tillage Res. 106, 344–348.
Becker, A., Klock, W., Friese, K., Schreck, P., Treutler, H.-C., Spettel, B., Duff, M.C., 2001. Lake Süber See as a natural sink for heavy metals Lake Su from copper mining. J. Geochem. Explor. 74, 205–217.
Bing, H., Wu, Y., Sun, Z., Yao, S., 2011. Historical trends of heavy metal contamination and their sources in lacustrine sediment from Xijiu Lake, Taihu Lake Catchment, China. J. Environ. Sci. 23, 1671–1678.
Blaauw, M., Christen, J.A., 2019. rbacon: Age-Depth Modelling Using Bayesian Statistics. R Package Version 2.3.7.
Boberg, F., Lundstedt, H., 2002. Solar wind variations related to fluctuations of the North Atlantic Oscillation. Geophys. Res. Lett. 29, 13–1.
Bonsal, B., Shabbar, A., 2011. Large-scale climate oscillations influencing Canada, 1900-2008. Canadian biodiversity: ecosystem status and trends 2010. In: Technical Thematic Report No. 4. Canadian Councils of Resource Ministers, Ottawa, Canada, pp. 1–15.
Bonsal, B.R., Shabbar, A., Higuchi, K., 2001. Impacts of low frequency variability modes on Canadian winter temperature. Int. J. Climatol. 21, 95–108.
Bonsal, B.R., Prowse, T.D., Duguay, C.R., Lacroix, M.P., 2006. Impacts of large-scale teleconnections on freshwater-ice break/freeze-up dates over Canada. J. Hydrol. 1, 340–353.
Bowell, R., Alpers, C., Jamieson, H., Nordstrom, D.K., Majzlan, J., 2014. The environmental geochemistry of arsenic: an overview. In: Reviews in Mineralogy and Geochemistry, Vol. 79. The Mineralogical Society of America, Virginia, USA.
Buermann, W., Anderson, B., Tucker, C.J., Dickinson, R.E., Lucht, W., Potter, C.S., Myneni, R.B., 2003. Interannual covariability in Northern Hemisphere air temperatures and greenness associated with El Niño-Southern Oscillation and the Arctic Oscillation. J. Geophys. Res. Atmos. 108, 1–16.
Bunn, A., Korpela, M., Biondi, F., Campelo, F., Mérian, P., Qeadan, F., Zang, C., Pucha-Cofrep, D., Wernicke, J., 2018. dplR: Dendrochronology Program Library in R. R Package Version 1.6.9.
Canadian Council of Ministers of the Environment, 2001. Canadian Water Quality Guidelines for the Protection of Aquatic Life: Arsenic.
Chang, A.S., Patterson, R.T., 2005. Climate shift at 4400 years BP: evidence from high-resolution diatom stratigraphy, Effingham Inlet, British Columbia, Canada. Palaeogeogr. Palaeoclimatol. Palaeoecol. 226, 72–92.
Christoforou, P., Hameed, S., 1997. Solar cycle and the Pacific "centers of action". Geophys. Res. Lett. 24 (3), 293–296.
Christoudias, T., Pozzer, A., Lelieveld, J., 2012. Influence of the North Atlantic Oscillation on air pollution transport. Atmos. Chem. Phys. 12, 869–877.
Chu, G., Sun, Q., Xie, M., Lin, Y., Shang, W., Zhu, Q., Shan, Y., Xu, D., Rioual, P., Wang, L., Liu, J., 2014. Holocene cyclic climatic variations and the role of the Pacific Ocean as recorded in varved sediments from northeastern China. Quat. Sci. Rev. 102, 85–95.
Cockburn, J.M.H., Lamoureux, S.F., 2008. Inflow and lake controls on short-term mass accumulation and sedimentary particle size in a High Arctic lake: implications for interpreting varved lacustrine sedimentary records. J. Paleolimnol. 40, 923–942.
Cuven, S., Francus, P., Lamoureux, S.F., 2010. Estimation of grain size variability with micro X-ray fluorescence in laminated lacustrine sediments, Cape Bounty, Canadian High Arctic. J. Paleolimnol. 44, 803–817.
Cuven, S., Francus, P., Lamoureux, S., 2011. Mid to Late Holocene hydroclimatic and geochemical records from the varved sediments of East Lake, Cape Bounty, Canadian High Arctic. Quat. Sci. Rev. 30, 2651–2665.
Dalton, A.S., Patterson, R.T., Roe, H.M., Macumber, A.L., Swindles, G.T., Galloway, J.M., Vermaire, J.C., Crann, C.A., Falck, H., 2018. Late Holocene climatic variability in Subarctic Canada: Insights from a high-resolution lake record from the Central Northwest Territories. PLoS One 13, 1–21.
Déry, S.J., Wood, E.F., 2005. Decreasing river discharge in northern Canada. Geophys. Res. Lett. 32, 1–4.
Deser, C., 2000. On the teleconnectivity of the "Arctic Oscillation". Geophys. Res. Lett. 27, 779–782.
Deser, C., Alexander, M.A., Xie, S., Phillips, A.S., 2009. Sea surface temperature variability: patterns and mechanisms. Annu. Rev. Mar. Sci. 2, 115–143.
Dickson, R.R., Osborn, T.J., Hurrell, J.W., Meincke, J., Blindheim, J., Adlandsvik, B., Vinje, T., Alekseev, G., Maslowski, W., 2002. The Arctic Ocean response to the North Atlantic Oscillation. J. Clim. 13, 2671–2696.
Eckhardt, S., Stohl, A., Beirle, S., Spichtinger, N., James, P., Forster, C., Junker, C., Wagner, T., Platt, U., Jennings, S.G., 2003. The North Atlantic Oscillation controls air pollution transport to the Arctic. Atmos. Chem. Phys. 3, 1769–1778.
Egozcue, J.J., Pawlowsky-Glahn, V., 2008. Simplicial geomtry for compositional data. Geol. Soc. Lond., Spec. Publ. 264 (1), 145–159.

Fauria, M.M., Johnson, E.A., 2006. Large-scale climatic patterns control large lightning fire occurrence in Canada and Alaska forest regions. J. Geophys. Res. Biogeosci. 111, 1–17.
Filzmoser, P., Hron, K., Reimann, C., 2009. Univariate statistical analisys of enviromental (compositional) data: problems and possibilities. Sci. Total Environ. 407 (23), 6100–6108.
Galloway, J.M., Wigston, A., Patterson, R.T., Swindles, G.T., Reinhardt, E., Roe, H.M., 2013. Climate change and decadal to centennial-scale periodicities recorded in a late Holocene NE Pacific marine record: examining the role of solar forcing. Palaeogeogr. Palaeoclimatol. Palaeoecol. 386, 669–689.
Galloway, J.M., Swindles, G.T., Jamieson, H.E., Palmer, M., Parsons, M.B., Sanei, H., Macumber, A.L., Patterson, R.T., Falck, H., 2018. Organic matter control on the distribution of arsenic in lake sediments impacted by ~ 65 years of gold ore processing in subarctic Canada. Sci. Total Environ. 622–623, 1668–1679.
Gavel, M.J., Patterson, R.T., Nasser, N.A., Galloway, J.M., Hanna, B.W., Cott, P.A., Roe, H.M., Falck, H., 2018. What killed Frame Lake? A precautionary tale for urban planners. PeerJ 6, e4850.
Gleissberg, W., 1971. The probable behaviour of sunspot cycle 21. Sol. Phys. 21, 240–245.
Gratz, L.E., Keeler, G.J., Miller, E.K., 2009. Long-term relationships between mercury wet deposition and meteorology. Atmos. Environ. 43, 6218–6229.
Gray, L.J., Beer, J., Geller, M., Haigh, J.D., Lockwood, M., Matthes, K., Cubasch, U., Fleitmann, D., Harrison, G., Hood, L., Luterbacher, J., Meehl, G.A., Shindell, D., van Geel, B., White, W., 2010. Solar influences on climate. Rev. Geophys. 48, RG4001.
Gray, L.J., Scaife, A.A., Mitchell, D.M., Osprey, S., Ineson, S., Hardiman, S., Butchart, N., Knight, J., Sutton, R., Kodera, K., 2013. A lagged response to the 11-year solar cycle in observed winter Atlantic/European weather patterns. J. Geophys. Res. Atmos. 118, 13405–13420.
Gray, L.J., Woollings, T.J., Andrews, M., Knight, J., 2016. Eleven-year solar cycle signal in the NAO and Atlantic/European blocking. Q. J. R. Meteorol. Soc. 142, 1890–1903.
Gregory, B.R.B., Patterson, R.T., Galloway, J.M., 2019a. Understanding the Impact of Millennial to Sub-Decadal Climate and Limnological Change on the Stability of Arsenic in Lacustrine Sediments. Unpublished PhD dissertation. Carleton University, Ottawa, ON, Canada.
Gregory, B.R.B., Patterson, R.T., Reinhardt, E.G., Galloway, J.M., 2019b. The iBox-FC: a new containment vessel for Itrax X-ray fluorescence core-scanning of freeze cores. Quat. Int. 514, 76–84.
Hodell, D.A., Brenner, M., Curtis, J.H., Guilderson, T., 2001. Solar forcing of drought frequency in the Maya Lowlands. Science 292, 1367–1370.
Hood, L.L., Soukharev, B.E., 2012. The lower-stratospheric response to 11-Yr. Solar forcing: coupling to the troposphere–ocean response. J. Atmos. Sci. 69, 1841–1864.
Hood, L., Schimanke, S., Spangehl, T., Bal, S., Cubasch, U., 2013. The surface climate response to 11-yr. solar forcing during northern winter: observational analyses and comparisons with GCM simulations. J. Clim. 26, 7489–7506.
Hu, F.S., Kaufman, D., Yoneji, S., Nelson, D., Shemesh, A., Huang, Y., Tian, J., Bond, G., Clegg, B., Brown, T., 2003. Cyclic variation and solar forcing of holocene climate inthe Alaskan Subarctic. Science 301, 1890–1893.
Hung, H., Blanchard, P., Halsall, C.J., Bidleman, T.F., Stern, G.A., Fellin, P., Muir, D.C.G., Barrie, L.A., Jantunen, L.M., Helm, P.A., Ma, J., Konoplev, A., 2005. Temporal and spatial variabilities of atmospheric polychlorinated biphenyls (PCBs), organochlorine (OC) pesticides and polycyclic aromatic hydrocarbons (PAHs) in the Canadian Arctic: results from a decade of monitoring. Sci. Total Environ. 342, 119–144.
Keimowitz, A.R., Zheng, Y., Chillrud, S.N., Mailloux, B., Jung, H.B., Stute, M., Simpson, H.J., 2005. Arsenic redistribution between sediments and water near a highly contaminated source. Environ. Sci. Technol. 39, 8606–8613.
Klein, W.H., 1949. The unusual weather and circulation of the 1948–1949 winter. Mon. Weather Rev. 77, 99–113.
Kodera, K., 2002. Solar cycle modulation of the North Atlantic Oscillation: implication in the spatial structure of the NAO. Geophys. Res. Lett. 29, 59–1.
Kodera, K., Kuroda, Y., 2002. Dynamical response to the solar cycle. J. Geophys. Res. 107, 1–12.
Kodera, K., Kuroda, Y., 2005. A possible mechanism of solar modulation of the spatial structure of the North Atlantic Oscillation. J. Geophys. Res. D Atmos. 110, 1–9.
Kraemer, B.M., Chandra, S., Dell, A.I., Dix, M., Kuusisto, E., Livingstone, D.M., Schladow, S.G., Silow, E., Sitoki, L.M., Tamatamah, R., McIntyre, P.B., 2017. Global patterns in lake ecosystem responses to warming based on the temperature dependence of metabolism. Glob. Chang. Biol. 23, 1881–1890.
Kren, A.C., Marsh, D.R., Smith, A.K., Pilewskie, P., 2016. Wintertime Northern Hemisphere response in the stratosphere to the Pacific decadal oscillation using the Whole Atmosphere Community Climate Model. J. Clim. 29, 1031–1049.
Lapointe, F., Francus, P., Lamoureux, S.F., Vuille, M., Jenny, J.P., Bradley, R.S., Massa, C., 2017. Influence of North Pacific decadal variability on the western Canadian Arctic over the past 700 years. Clim. Past 13, 411–420.
Lean, J., Rottman, G., Harder, J., Kopp, G., 2005. SORCE contributions to new understanding of global change and solar variability. In: Sol Radiat Clim Exp Mission Descr Early Results, pp. 27–53.
Liu, X., Rao, Z., Shen, C.C., Liu, J., Chen, J., Chen, S., Wang, X., Chen, F., 2019. Holocene solar activity imprint on centennial- to multidecadal-scale hydroclimatic oscillations in arid Central Asia. J. Geophys. Res. Atmos. 124, 2562–2573.
Loseto, L.L., Stern, G.A., Macdonald, R.W., 2015. Distant drivers or local signals: where do mercury trends in western Arctic belugas originate? Sci. Total Environ. 510, 226–236.
Macdonald, R.W., Harner, T., Fyfe, J., 2005. Recent climate change in the Arctic and its impact on contaminant pathways and interpretation of temporal trend data. Sci. Total Environ. 342, 5–86.
MacDonald, G.M., Porinchu, D.F., Rolland, N., Kremenetsky, K.V., Kaufman, D.S., 2009. Paleolimnological evidence of the response of the Central Canadian treeline zone to radiative forcing and hemispheric patterns of temperature change over the past 2000 years. J. Paleolimnol. 41, 129–141.
Macumber, A.L., Patterson, R.T., Galloway, J.M., Falck, H., Swindles, G.T., 2018. Reconstruction of Holocene hydroclimatic variability in subarctic treeline lakes using lake sediment grain-size end-members. The Holocene 28 (6), 845–857.
Mantua, N.J., Hare, S.R., 2002. The Pacific Decadal Oscillation. J. Oceanogr. 58, 35–44.
Martin, A.J., Pedersen, T.F., 2002. Seasonal and interannual mobility of arsenic in a lake impacted by metal mining. Environ. Sci. Technol. 36, 1516–1523.
Massei, N., Durand, A., Deloffre, J., Dupont, J.P., Valdes, D., Laignel, B., 2007. Nvestigating possible links between the North Atlantic oscillation and rainfall variability in northwestern France over the past 35 years. J. Geophys. Res. 112, 1–10.
McCurdy, M.W., McNeil, R.J., 2014. Geological Survey of Canada open file 7577. In: Geochemical Data from Stream Silts and Surface Waters in the Pine Point Mining District, Northwest Territories (NTS 85-B).
McGregor, H.V., Gagan, M.K., 2004. Western Pacific coral δ18O records of anomalous Holocene variability in the El Niño-Southern Oscillation. Geophys. Res. Lett. 31, 1–4.
Meehl, G.A., Arblaster, J.M., Branstator, G., 2008. A coupled air-sea response mechanism to solar forcing in the Pacific region. J. Clim. 21, 2883–2897.
Meehl, G.A., Arblaster, J.M., Matthes, K., Sassi, F., van Loon, H., 2009. Amplifying the pacific climate system response to a small 11-year solar cycle forcing. Science 325, 1114–1118.
Miller, C.B., Parsons, M.B., Jamieson, H.E., Swindles, G.T., Nasser, N.A., Galloway, J.M., 2019. Lake-specific controls on the long-term stability of mining-related, legacy arsenic contamination and geochemical baselines in a changing northern environment, Tundra Mine, Northwest Territories, Canada. Appl. Geochem. 109, 104403.
Miller, C.B., Parsons, M.B., Jamieson, H.E., Ardakani, O.H., Gregory, B.R.B., Galloway, J. M., 2020. Influence of late Holocene climate on solid-phase speciation and long-term stability of arsenic in sub-Arctic lake sediments. Sci. Total Environ. 709, 136115.
Misios, S., Mitchell, D.M., Gray, L.J., Tourpali, K., Matthes, K., Hood, L., Schmidt, H., Chiodo, G., Thiéblemont, R., Rozanoc, E., Krivolutsky, A., 2016. Solar signals in CMIP-5 simulations: effects of atmosphere-ocean coupling. Q. J. R. Meteorol. Soc. 142, 928–941.
Misios, S., Gray, L.J., Knudsen, M.F., Karoff, C., Schmidt, H., Haigh, J.D., 2019. Slowdown of the Walker circulation at solar cycle maximum. Proc. Natl. Acad. Sci. 116, 7186–7191.
Moore, J.C.G., 1986. Courageous-Matthews Lake area, district of MacKenzie, Northwest Territories. In: Geological Survey of Canada Department of Mines and Technical surveys Report # 2524.
Moy, C., Seltzer, G., Rodbell, D., Anderson, D., 2002. Variability of El Niño/Southern Oscillation activity at millennial timescales during the Holocene epoch. Nature 420, 162–165.
Nasser, N.A., Patterson, R.T., Roe, H.M., Galloway, J.M., Falck, H., Sanei, H., 2020. Use of Arcellinida (testate lobose amoebae) arsenic tolerance limits as a novel tool for biomonitoring arsenic contamination in lakes. Ecol. Indic. 113, 106177.
Newman, M., Alexander, M.A., Ault, T.R., Cobb, K.M., Deser, C., Lorenzo, E.D., Mantua, N.J., Miller, A.J., Minobe, S., Nakamura, H., Schneider, N., Vimont, D.J., Phillips, A.S., Scott, J.D., Smith, C.A., 2016. The Pacific decadal oscillation, revisited. J. Clim. 29, 4399–4427.
Ogurtsov, M.G., Nagovitsyn, Y.A., Kocharov, G.E., Jungner, H., 2002. Long-period cycles of the Sun's activity recorded in direct solar data and proxies. Sol. Phys. 211, 371–394.
Ólafsdóttir, K.B., Geirsdóttir, Á., Miller, G.H., Larsen, D.J., 2013. Evolution of NAO and AMO strength and cyclicity derived from a 3-ka varve-thickness record from Iceland. Quat. Sci. Rev. 69, 142–154.
Osterberg, E.C., Mayewski, P.A., Fischer, D.A., Kreutz, K.J., Maasch, K.A., Sneed, S.B., Kelsey, E., 2014. Mount Logan ice core record of tropical and solar influences on Aluetian Low variability: 500-1998 A.D. J. Geophys. Res. 119 (11), 1–8.
Outridge, O.M., Sanei, H., Stern, G.A., Hamilton, P.B., Goodarzi, P., 2007. Evidence for control of Mercury accumulation rates in Canadian high Arctic lake sediments by variations of aquatic primary productivity. Environ. Sci. Technol. 41 (15), 5259–5265.
Padgham, W.A., 1992. Mineral deposits in the Archean Slave Structural Province; lithological and tectonic setting. Precambrian Res. 58, 1–24.
Palmer, M.J., Chetelat, J., Richardson, M., Jamieson, H.E., Galloway, J.M., 2019. Seasonal variation of arsenic and antimony in surface waters of small subarctic lakes impacted by legacy mining pollution near Yellowknife, NT, Canada. Sci. Total Environ. 684, 326–339.
Park, J., 2017. Solar and tropical ocean forcing of late-Holocene climate change in coastal East Asia. Palaeogeogr. Palaeoclimatol. Palaeoecol. 469, 74–83.
Patterson, R.T., Prokoph, A., Chang, A.S., 2004a. Late Holocene sedimentary response to solar and cosmic ray activity influenced climate variability in the NE Pacific. Sediment. Geol. 172 (2), 67–84.
Patterson, R.T., Prokoph, A., Wright, C., Chang, A.S., Thomson, R.E., Ware, D.M., 2004b. Holocene solar variability and pelagic fish productivity in the NE Pacific. Palaeontol. Electron. 7, 1–17.
Patterson, R.T., Prokoph, A., Kumar, A., Chang, A.S., Roe, H.M., 2005. Holocene variability in pelagic fish and phytoplankton productivity along the west coast of Vancouver Island, NE Pacific Ocean. Mar. Micropaleontol. 55 (4), 183–204.
Patterson, R.T., Prokoph, A., Reinhardt, A., Roe, H.M., 2007. Climate cyclicity in late Holocene anoxic marine sediments from the Seymour-Belize Inlet Complex, British Columbia. Quaternary Land-Ocean Interactions: sea-Level Change, Sediments and Tsunami. Mar. Geol. 242 (3), 123–140.

Patterson, R.T., Chang, A.S., Prokoph, A., Roe, H.M., Swindles, G.T., 2013. Influence of the Pacific Decadal Oscillation, El Niño-Southern Oscillation and solar forcing on climate and primary productivity changes in the Northeast Pacific. Quat. Int. 310, 124–139.
Pena, J.C., Schulte, L., Badoux, A., Barriendos, M., Barrera-Escoda, A., 2015. Influence of solar forcing, climate variability and modes of low-frequency atmospheric variability on summer floods in Switzerland. Hydrol. Earth Syst. Sci. 19, 3807–3827.
Quesada, A., Vincent, W.F., Kaup, E., Hobbie, J.E., Laurion, I., 2006. Landscape control of high latitude lakes in a changing climate. In: Trends in Antarctic Terrestrial and Limnetic Ecosystems: Antarctica as a Global Indicator, pp. 221–252.
R Core Team, 2019. R: A Language and Environment for Statistical Computing. R Foundation for Statistical Computing, Vienna, Austria.
Raspopov, O.M., Dergachev, V.A., Esper, J., Kozyreva, O.V., Frank, D., Ogurtsov, M., Kolstrom, T., Shao, X., 2008. The influence of the de Vries (~200-year) solar cycle on climate variations: results from the Central Asian Mountains and their global link. Palaeogeogr. Palaeoclimatol. Palaeoecol. 259, 6–16.
Reimer, P.J., Bard, E., Bayliss, A., Beck, J.W., Blackwell, P.G., Ramsey, C.B., Buck, C.E., Cheng, H., Edwards, R.L., Friedrich, M., Grootes, P.M., Guilderson, T.P., Haflidason, H., Hajdas, I., Hatte, C., Heaton, T.J., Hoffman, D.L., Hogg, A.G., Hughen, K.A., Kaiser, K.F., Kromer, B., Manning, S.W., Niu, M., Reimer, R.W., Richards, D.A., Scott, E.M., Southon, J.R., Staff, R.A., Turney, C.S.M., ven der Plicht, J., 2013. IntCal13 and Marine13 Radiocarbon age calibration curves 0-50,000 years cal. yr. BP. Radiocarbon 55, 1869–1887.
Rigét, F., Vorkamp, K., Hobson, K.A., Muir, D.C.G., Dietz, R., 2013. Temporal trends of selected POPs and the potential influence of climate variability in a Greenland ringed seal population. Environ. Sci. Process Impacts 15, 1706–1716.
Rossi, A., Massei, A., Laignel, B., 2011. A synthesis of the time-scale variability of commonly used climate indices using continuous wavelet transform. Glob. Planet. Chang. 78, 1–13.
Roy, I., Haigh, J.D., 2010. Solar cycle signals in sea level pressure and sea surface temperature. Atmos. Chem. Phys. 10, 3147–3153.
Roy, I., Haigh, J.D., 2012. Solar cycle signals in the pacific and the issue of timings. J. Atmos. Sci. 69, 1446–1451.
Rydberg, J., Klaminder, J., Rosén, P., Bindler, R., 2010. Climate driven release of carbon and mercury from permafrost mires increases mercury loading to sub-arctic lakes. Sci. Total Environ. 408, 4778–4783.
Sarmiento, S., Palanisami, A., 2011. Coherence between atmospheric teleconnections and Mackenzie River Basin lake levels. J. Great Lakes Res. 37, 642–649.
Scaife, A.A., Ineson, S., Knight, J.R., et al., 2013. A mechanism for lagged North Atlantic climate response to solar variability. Geophys. Res. Lett. 40, 434–439.
Schuh, C.E., Jamieson, H.E., Palmer, M.J., Martin, A.J., 2018. Solid-phase speciation and post-depositional mobility of arsenic in lake sediments impacted by ore roasting at legacy gold mines in the Yellowknife area, Northwest Territories, Canada. Applied Geochemistry 91, 208–220.
Schulz, M., Mudelsee, M., 2002. REDFIT: estimating red-noise spectra directly from unevenly spaced paleoclimatic time series. Comput. Geosci. 28, 421–426.
Seabridge Gold Inc, 2010. Courageous Lake Project Description in Support of a Class " A " Land Use Permit (Former Permit MV2003C0050).
Sheffield, J., Wood, E.F., 2008. Global trends and variability in soil moisture and drought characteristics, 1950-2000, from observation-driven simulations of the terrestrial hydrologic cycle. J. Clim. 21, 432–458.
Shen, C., Wang, W.C., Gong, W., Hao, Z., 2006. A Pacific Decadal Oscillation record since 1470 AD reconstructed from proxy data of summer rainfall over eastern China. Geophys. Res. Lett. 33, 1–4.
Silke, R., 2009. The Operational History of Mines in the Northwest Territories, Canada.
Simpson, I.R., Blackburn, M., Haigh, J.D., 2009. The role of eddies in driving the tropospheric response to stratospheric heating perturbations. J. Atmos. Sci. 66, 1347–1365.
Sinha, E., Michalak, A.M., Balaji, V., 2017. Eutrophication will increase during the 21st century as a result of precipitation changes. Science 357, 1–5.
Skinner, W.R., Shabbar, A., Flannigan, M.D., Logan, K., 2006. Large forest fires in Canada and the relationship to global sea surface temperatures. J. Geophys. Res. Atmos. 111, 1–14.
Slemr, F., Brenninkmeijer, C.A., Rauthe-Schöch, A., Weigelt, A., Ebinghaus, R., Brunke, E.-G., Martin, L., Spain, T.G., O'Doherty, S., 2016. El Niño-Southern Oscillation influence on tropospheric mercury concentrations. Geophys. Res. Lett. 43, 1766–1771.
Smith, D.M., Scaife, A.A., Eade, R., Knight, J.R., 2016. Seasonal to decadal prediction of the winter North Atlantic Oscillation: emerging capability and future prospects. Q. J. R. Meteorol. Soc. 142, 611–617.
Snortheim, C.A., Hanson, P.C., McMahon, K.D., Read, J.S., Carey, C.C., Dugan, H.A., 2017. Meteorological drivers of hypolimnetic anoxia in a eutrophic, north temperate lake. Ecol. Model. 343, 39–53.
Solanki, S.K., Usoskin, I.G., Kromer, B., Schüssler, M., Beer, J., 2004. Unusual activity of the Sun during recent decades compared to the previous 11,000 years. Nature 431 (7012), 1084–1087.
Suess, H.E., 1980. The radiocarbon record in tree rings of the last 8000 years. Radiocarbon 22, 200–209.
Suess, H.E., 1986. Secular variations of cosmogenic 14C on Earth: their discovery and Interpretation. Radiocarbon 28, 259–265.
Tetra Tech Wardrop, 2012. Courageous Lake Prefeasibility Study, pp. 1–450.
Thiéblemont, R., Matthes, K., Omrani, N.E., Kodera, K., Hansen, F., 2015. Solar forcing synchronizes decadal North Atlantic climate variability. Nat. Commun. 6, 1–8.
Thompson, P.H., Kerswill, J.A., 1994. Preliminary Geology of the Winter Lake – Lac de Gras area, District of MacKenzie, Northwest Territories, Open File 2740 (Revised), Scale 1:250000.
Thompson, D.W.J., Wallace, J.M., 1998. The Arctic Oscillation signature in the wintertime geopotential height and temperature fields. Geophys. Res. Lett. 25, 1297–1300.
Timoney, K., Peterson, G., Fargey, P., Peterson, M., McCanny, S., Wein, R., 1997. Spring ice-jam flooding of the Peace-Athabasca Delta: evidence of a climatic oscillation. Clim. Chang. 35, 463–483.
Torrence, C., Compo, G.P., 1998. A practical guide to wavelet analysis. Bull. Am. Meteorol. Soc. 79, 61–78.
Van den Berghe, M.D., Jamieson, H.E., Palmer, M.J., 2018. Arsenic mobility and characterization in lakes impacted by gold ore roasting, Yellowknife, NWT, Canada. Environ. Pollut. 234, 630–641.
Van Loon, H., Meehl, G.A., 2008. The response in the Pacific to the sun's decadal peaks and contrasts to cold events in the southern oscillation. J. Atmos. Solar-Terr. Phys. 70, 1046–1055.
Van Loon, H., Meehl, G.A., 2011. The average influence of decadal solar forcing on the atmosphere in the South Pacific region. Geophys. Res. Lett. 38, 1–5.
Van Loon, H., Meehl, G.A., 2016. Interactions between externally forced climate signals from sunspot peaks and internally generated Pacific Decadal and North Atlantic Oscillations. Geophys. Res. Lett. 41 (1), 161–166.
Van Loon, H., Rogers, J.C., 1978. The Seesaw in Winter Temperatures between Greenland and Northern Europe. Part I: General Description. Mon. Weather Rev. 106, 296–310.
Van Loon, H., Brown, J., Milliff, R.F., 2012. Trends in sunspots and North Atlantic Sea level pressure. J. Geophys. Res. Atmos. 117, 1–8.
Veretenenko, S., Ogurtsov, M., 2019. Manifestation and possible reasons of ~60-year oscillations in solar-atmospheric links. Adv Sp Res 64, 104–116.
Vincent, L.A., Zhang, X., Brown, R.D., Feng, Y., Mekis, E., Milewska, E.J., Wan, H., Wang, X.L., 2015. Observed trends in Canada's climate and influence of low-frequency variability modes. J. Clim. 28, 4545–4560.
Wang, C., Picaut, J., 2004. Understanding ENSO physics—a review. In: Geophysical Monograph Series, pp. 21–48.
Wang, Y., Cheng, H., Edwards, R.L., He, Y., Kong, X., An, Z., Wu, J., Kelly, M.J., Dykoski, C.A., Li, X., 2005. The Holocene Asian monsoon: links to solar changes and North Atlantic climate. Science 308, 854–857.
Wanner, H., Bronnimann, S., Casty, C., Gyalistras, D., Luterbacher, J., Schmutz, C., Stephenson, D.B., Xoplaki, E., 2001. North Atlantic Oscillation – concepts and studies. Surv. Geophys. 22, 321–382.
Weltje, G.J., Bloemsma, M.R., Tjallingii, R., Heslop, D., Röhl, U., Croudace, I.W., 2015. Prediction of geochemical composition from XRF core scanner data: a new multivariate approach including automatic selection of calibration samples and quantification of uncertainties. In: Micro-XRF Studies of Sediment Cores: Applications of a Non-Destructive Tool for Environmental Sciences: Part III.
Wetzel, R., 2001. Limnology: Lake and River Ecosystems, 3rd ed. Gulf professional publishing.
Wiles, G.C., D'Arrigo, R.D., Villalba, R., Calkin, P.E., Barclay, D.J., 2004. Century-scale solar variability and Alaskan temperature change over the past millennium. Geophys. Res. Lett. 31, 2–5.
Xu, D., Lu, H., Chu, G., Wu, N., Shen, C., Wang, C., Mao, L., 2015. 500-year climate cycles stacking of recent centennial warming documented in an East Asian pollen record. Sci. Rep. 4, 1–7.
Zhang, X., Wang, J., Zwiers, F.W., Groisman, P.Y., 2010. The influence of large-scale climate variability on winter maximum daily precipitation over North America. J. Clim. 23, 2902–2915.
Zhang, W., Niu, J., Ming, Q., Shi, Z., Lei, G., Huang, L., Long, X., Chang, F., 2018. Holocene climatic fluctuations and periodic changes in the Asian southwest monsoon region. J. Asian Earth Sci. 156, 90–95.